JOURNAL OF GEOPHYSICAL RESEARCH, VOL. 106, NO. B8, PAGES 16,461–16,481, AUGUST 10, 2001

Erosion and rheology controls on synrift and postrift evolution: Verifying old and new ideas using a fully coupled numerical model

E. Burov

Laboratoire Téctonique ESA 7072, Université de Pierre et Marie Curie, Paris, France

A. Poliakov

Laboratoire de Géophysique, Téctonique et Sédimentologie UMR 5573, CNRS - Université de Montpellier, Montpellier, France

Abstract. We use a fully coupled asymmetric dynamic finite element model to study interactions between thermomechanical behavior and surface processes during continental rift evolution. The model accounts for (1) nonlinear brittle-elastic-ductile rheology, layered lithological structure, and faulting; (2) heat transport and thermal buoyancy forces; and (3) "true" erosion and sedimentation (grid elements are eliminated and recreated). Faults are not predefined but are self-localized; their distributions and geometry are model outputs, which provides new geologically sensible constraints on its validity. We test previous ideas on rift evolution based on numerical and analytical component theories (or individual parts) of our model. After demonstrating that our coupled model reproduces classic rift features, we then demonstrate that synrift surface processes result in enhanced lithospheric thinning and widening of the basin, so that the apparent stretching factors increase by a factor of 1.5–2. Sedimentation results not only in thermal but also in localized flexural weakening of the lithosphere, which locally compensates strengthening due to cooling. Erosion on the uplifted flanks produces local strengthening and rebound. Surface processes produce pressure gradients, which drive a ductile crustal flow that (1) provides a fast feedback with tectonic processes and controls subsidence rates and flank stability and (2) drives a secondary extension or compression and uplift on the late synrift/early postrift phase. Our results indicate that kinematic and dynamic rift models that ignore erosion may produce misleading results in many rifts. We reproduced and explained a number of enigmatic synrift phenomena, such as (1) polyphase subsidence provoked by switching of the level of necking between different competent lithological layers and (2) synrift and postrift stagnation and vertical accelerations unassociated with tectonic stress inversion or phase changes.

1. Introduction

Rift evolution is a coupled problem where thermal and mechanical processes closely interact. The interaction of these processes with surface erosion and sedimentation is much less studied because most of the existing kinematic and dynamic basin models focused on thermomechanical processes and ignored synrift and postrift surface processes. Most of early rift modelers have considered only thermomechanical processes [e.g., *England*, 1983; *Kusznir et al.*, 1987; *Dunbar and Sawyer*, 1988; *Watts and Torne*, 1992; *Chery et al.*, 1992; *Bassi*, 1995; *Hopper and Buck*, 1996]. Others have focused their studies on surface processes only and, at best, coupled them with simple isostatic reaction using equivalent forces instead of true erosion/sedimentation [*Ebinger et al.*, 1991; *Kooi and Beaumont*, 1994; *van der Beek et al.*, 1995; *van Balen et al.*, 1995; *Burov and Cloetingh*, 1997]. In addition, many studies have also investigated the importance of secondary effects of erosion and sedimentation such as retarded cooling due to thermal blanketing in a type of sensitivity analysis [e.g., *England and Richardson*, 1980; *Stephenson et al.*, 1989; *Lobkosvsky and Kerchman*, 1992]. Although formation and evolution of the border faults are major factors of rift evolution, none of the previous coupled models allowed faults to form, rather than a priori specifying their locations.

Effects of coupling between the surface and subsurface processes (apart of simple elastic flexure) were investigated in only a few semianalytical models: *Burov and Cloetingh* [1997] studied the influence of surface processes during the postrift phase using a small strain multilayer model with nonlinear rheology, which neglected faulting; *Poliakov et al.* [2001] conducted a simplified complementary analytical study of synrift erosion.

At close consideration, it appears to be invalid to ignore surface processes in mechanical models. The former produce and laterally redistribute normal loads of 50 to 500 MPa; that is of the same order as the tectonic forces (5-22 km of sediments over 50-200 km horizontal distances, e.g., Pannonian basin, Albert rift, Baikal rift, Dnieper-Donetz basin [e.g.,

Paper number 2001JB000433.
0148-0227/01/2001JB000433$09.00

Burov and Cloetingh, 1997]). Erosion "follows" the tectonic deformation because its rates are strongly dependent on local topography heights and slopes [*van der Beek* et al., 1995; *van Balen et al.*, 1995; *Burov and Cloetingh*, 1997]. In contrast to inherent assumptions implied in common models [e.g., *McKenzie*, 1978], surface depressions cannot be automatically filled with sediment because the infill rates and sedimentary volumes are limited by the production capacity of the flank erosion and by the transport capacity of the fluvial network. The latter depend on many factors such as regional climate and soil type and may be insufficient or excessive resulting in different mechanical responses of the system to equivalent tectonic inputs.

As was first suggested by *Lobkovsky and Kerchman* [1992], sedimentational and erosional loading/unloading may drive flow in the ductile crust (Figures 1c and 1b). Further developing this idea, one can suggest that erosional removal of the uppermost cold strong brittle material must be compensated at depth by uplift of a weaker ductile material (Figure 1a), resulting in thinning and thus in easier extension of the strong upper crustal layer. Following *Burov and Cloetingh* [1997], one can also suggest that the inelastic flexure and yielding under sedimentary load should lead to (1) more localized depression in the middle of the basin; (2) enhanced extension due to reduction of the lithospheric resistance; (3) maintenance of high strength beneath the flanks; and (3) formation of secondary zones of flexural weakening just outside the flanks (Figure 1b and *Burov and Cloetingh* [1997]). These effects are actually observed [e.g., *Ebinger et al.*, 1989, 1999] and, naturally, should influence subsidence phases inferred from tectonic geomorphology and fission track age/length patterns [*Rohrman et al.*, 1995].

Previous models have considered only separate pieces of the "tectonics/surface processes/faulting" puzzle. In the present study, we combine a state-of-the-art model of thermomechanical and surface processes to investigate influence of the latter on both synrift and postrift evolution, with primary accent on their interplay with ductile flow and faulting during the synrift phase. Our second goal is to test the relative importance of some previous ideas, such as those of postrift strengthening due to cooling [e.g., *England*, 1983] and of its possible compensation by thermal blanketing [*Stephenson et al.*, 1989] and flexural weakening [*Burov and Cloetingh*, 1997]. For that we modified the finite element method (FEM) code Parovoz [*Poliakov et al.*, 1993], which handles previously unaccounted brittle strain localization (faulting) and "true" surface erosion (the grid elements are really "eroded" and "deposited" with appropriate changes in physical properties). Common limitations of the previous models are also circumvented through incorporation of nonlinear brittle-elastic-ductile rheology, rift asymmetry, thermal transport, and thermal buoyancy forces.

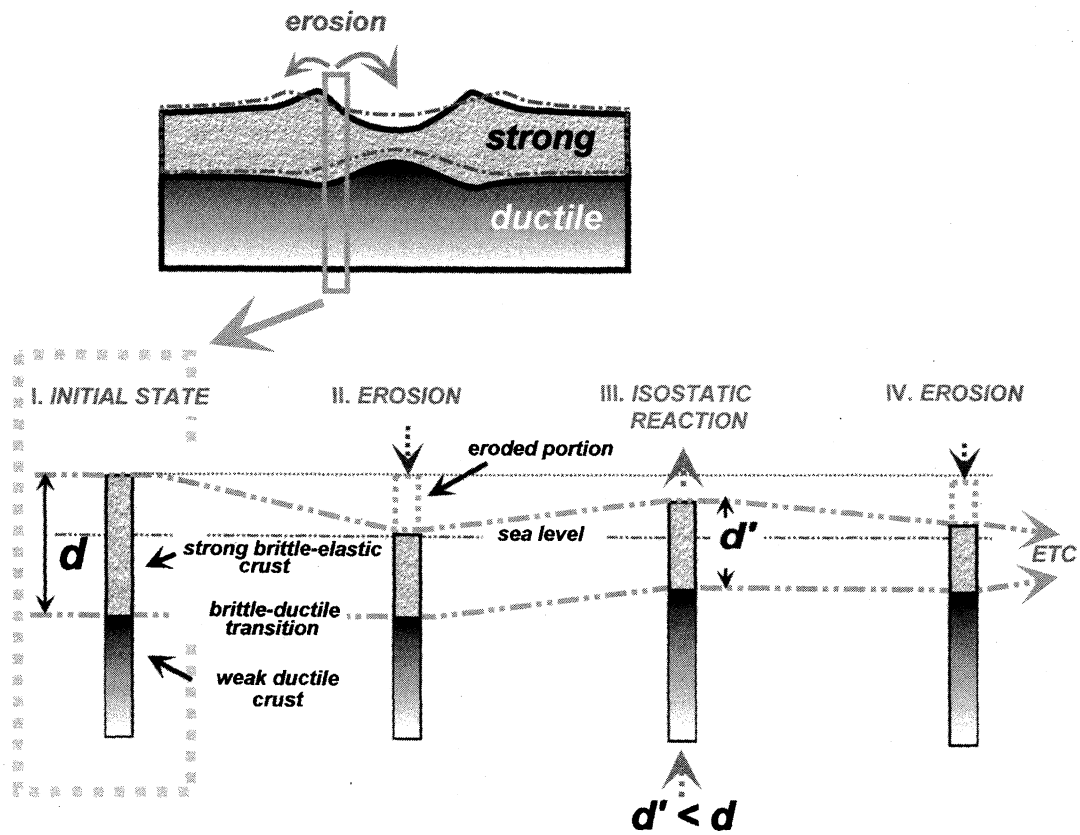

Figure 1a. Erosion and tectonic response, illustration of basic ideas. Simplified cartoon (local isostasy) explaining short-term weakening and thinning of crust resulting from erosion and isostatic reaction. Here *d* and *d'* are the thicknesses of a strong crustal layer before and after a single erosion/reaction cycle, respectively. Erosion removes uplifted topography, which results in reduction of the thickness of the strong crustal layer. This removal is partly compensated by isostatic uplift of the ductile material, but the thickness of the strong layer is vanishing. Thus when extension is applied, erosion will ease extensional thinning.

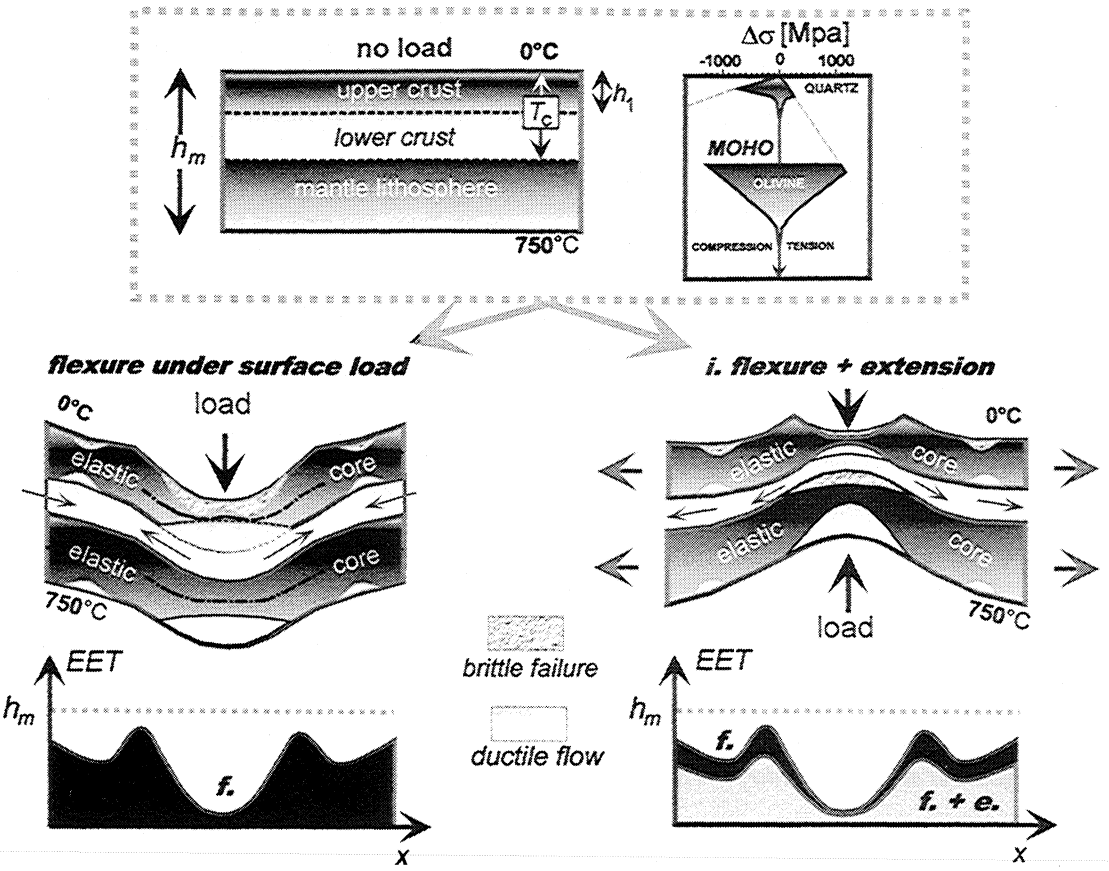

Figure 1b. Role of nonlinear continental rheology (yield-stress envelope, left) in flexural deformation under surface load and tensional stress (after analytical models of *Burov and Diament* [1996] and *Burov and Cloetingh* [1997]). Bending stress results in strong localized inelastic yielding in areas of maximal flexure and consequently in strong weakening (reduction of the integrated strength, or effective elastic thickness (EET), curve *f*) of the lithosphere below the sedimentary load and outside of the flanks. This weakening may be as important as that due to extension (*e*). Note secondary flexural weakening zones outside the rift flanks.

2. Fully Coupled Threefold Thermomechanical Model of Synrift and Postrift Basin Evolution

2.1. How It May Work? Basic Ideas

Erosion is a selective process that first acts on "fresh" (i.e., rough, steep) growing topography. If the topography growth accelerates, erosion rate accelerates too; if the topography flattens, the erosion rate goes down as well. Rift flanks, pop-up structures, and tilted blocks resulting from tectonic extension are thus the first targets of erosion. In a mechanically balanced system, removal (unloading) of uplifted topography must drive a compensatory (e.g., isostatic) rock uplift. This uplift occurs at the expense of near surface strong cold brittle crustal material and of hotter ductile material at depth. Most rift systems are characterized by elevated heat flow imposing temperatures higher than 300°C at 15 km depth and 600°C at Moho depth, which suggests that granite upper crust and even more basic lower crust must be ductile [*Carter and Tsenn*, 1987; *Brace and Kohlstedt*,1980]. Consequently, removal of strong surface material is balanced by uplift of a much weaker matter from below, which means that the competent part of the upper crust vanishes without extension (Figures 1a and 1b). This nonextensional erosional thinning of the competent crustal layer facilitates the "job" of the extensional tectonic or asthenospheric forces (Figures 1b and 1c).

According to the simplified postrift model by *Burov and Cloetingh* [1997] the upflow of the ductile crust must be strongest in the flank area because it is enforced by lateral outflow from under the middle of the basin. This outflow is provoked by local pressure rise induced by the developing sedimentary load and rift necking: As the ductile crustal channel thins under the center of the basin, the ductile crust gets laterally squeezed outward (Figure 1c). If necking and sedimentation become insufficient to force outward crustal flow, the crust will flow back, i.e., from the flanks to the middle of the basin. Dynamic pressure differences in the ductile crust resulting from erosion/sedimentation (10-50 MPa [*Burov and Cloetingh*, 1997; *Bertotti et al.*, 2000]) are high enough to override other contributions to nonhydrostatic pressure (Figure 1c). One can also hypothesize that for a shallow level of necking, the basin should primarily subside into the ductile crust during the initial stages of rifting. If significant "intracrustal" subsidence occurs, the induced ductile crustal flow will compete with the background tectonic flow. Consequently, this flow will provide an effective feedback between the surface and subsurface processes.

2.2. Threefold Large Strain Numerical Implementation

The interplay between surface and subsurface loads and forces is treated in our threefold (surface processes, mechanical behavior, heat transfer) fully coupled numerical algorithm Parovoz developed with large involvement of Y. Podladchikov [*Poliakov et al.*, 1993]. Parovoz is a hybrid finite element/finite differences fully explicit time-marching Lagrangian algorithm derived from the widely known FLAC algorithm (see *Cundall* [1989] and Appendix A for details). The new modifications include (1) the erosion/sedimentation model from *Burov and Cloetingh* [1997]; (2) rheological and lithological model from *Burov and Cloetingh* [1997]; (3) heat advection and conduction including initial age-dependent temperature field [*Burov and Diament*, 1995; *Lavier et al.*, 2000]. Parovoz handles rheologically complex behaviors in large strain mode (Appendix A), including localization and propagation of nonpredefined faults (shear bands), power law creep, and various kinds of strain-softening and work-hardening behaviors [see also *Buck and Poliakov*, 1998; *Burov and Molnar*, 1998; *Gerbault et al.*, 1999; *Burov and Guillou-Frottier*, 1999].

2.3. Surface Processes

Surface load evolution is described through diffusion-like erosion laws and fluvial transport laws [*Gossman*, 1976; *Kirkby*, 1986; *Willgoose et al.*, 1991; *Leeder*, 1991; *Beaumont et al.*, 1992]:

Slope erosion $dh/dt = k^*(x,h,\nabla h)\,\nabla^2 h,$ (1)

Fluvial transport $q_{fe}=-K_f q_r dh/dl,$ (2)

where h is topography, t is time, x is horizontal coordinate, k^* is experimentally established scale-dependent coefficient of erosion, q_r is river discharge, dh/dl is the slope in the direction of the river drainage, q_{fe} is material flux due to fluvial transport, K_f is a nondimensional transport coefficient, and l is the distance along the transporting channel. For nonlinear erosion laws, called first- second- and third-order erosion laws, k^* is a function of the first, second or third power, respectively, of the topography gradient [e.g., *Kooi and Beamont*, 1994]. For simplicity, we used zero-order linear diffusion (k^* is constant) for the short-range erosion and flat deposition for long-range fluvial transport below 100 m [*Avouac and Burov*, 1996]. It should be noted that assumption of conservation of matter would require that the slope erosion law (1) takes form

$$dh/dt = \mathrm{div}[k^*(x,h,\nabla h)\,\nabla h\,]. \quad (3)$$

Yet the slope law (1) is derived empirically and thus only resembles diffusion law in case of nonconstant coefficient of erosion [e.g., *Gossman*, 1976]. In this case the difference between this law and classical diffusion reflects unaccounted material loss from the system.

2.4. Rheology

In contrast to classical studies [e.g., *Dunbar and Sawyer*, 1988], which used linear rheologies to fit desired rheological yield-stress envelopes, we implicitly use the nonlinear brittle-elasto-ductile rheology laws from *Brace and Kohlstedt* [1980], *Carter and Tsenn* [1987], *Kirby and Kronenberg* [1987], *Kohlstedt et al.* [1995], and *Ranalli* [1995]. We assume quartz-dominated upper crust, quartz-diorite or quartz-controlled lower crust, and olivine-dominated mantle (Figures 1b and 1c). The ductile behavior is presented by power law creep: $\dot{\varepsilon} = A_0 \exp(-H^*/RT)\,(\sigma_1-\sigma_3)^n$, where $\dot{\varepsilon}$ is strain rate, T is temperature, σ_1 and σ_3 are the principal stresses, $A_0, H^*, R,$ and n are the material constants explained in Table 1. The brittle part is given by Byerlee's law [*Ranalli*, 1995] approximated by Mohr-Coulomb plasticity with friction angle 30° and cohesion of 20 MPa. The elastic part is defined using commonly inferred values of elastic constants for lithospheric rocks [*Turcotte and Schubert*, 1982] (Table 1).

Subsidence of a basin is largely controlled by its integrated flexural strength. It must be noted that this strength (often expressed in terms of equivalent elastic thickness of the lithosphere, EET) cannot be evaluated from simple summation of the respective strengths of each rheological layer if some of the layers are mechanically decoupled from each other. The EET of a totally decoupled layered system is ~2-3 times smaller than that of a coupled one. The EET of a decoupled system can be roughly estimated as $\mathrm{EET} = (\Sigma h_i^3)^{1/3}$, compared to simply Σh_i for a coupled one, where h_i is the thickness of ith competent rheological layer [*Burov and Diament*, 1995]. This effect should be kept in mind in relation with the following description of the experiments and discussion of the results.

2.5. Boundary and Initial Conditions

The boundary conditions include constant lateral velocity, free upper surface and pliable Winkler basement [*Burov and Cloetingh*, 1997]. The numerical mesh is rectangular and composed of 62,500 to 125,000 quadruple elements each constructed of two couples of overlapped triangular elements [*Cundall*, 1989]. The initial thermal structure is defined from the thermotectonic age (age of the last large-scale thermal event) of the lithosphere before rifting, calculated from the half-space model given by *Burov and Diament* [1995]. Following *Chery et al.* [1992], a small (100°C) Gaussian shaped temperature anomaly at the bottom is used as the initial perturbation. Other parameters are given in Table 1. The size of computing area varies from 80 km × 20 km for young hot lithosphere to 500 km × 150 km for old cold lithosphere.

3. Experiments and Results

We varied three major parameters: (1) initial thermo-tectonic age (t_a), varied from young (50 Ma) to middle (250 Ma) and old (400 Ma); (2) rifting phase duration, varied from short, 1.5 Myr, to long, 7 Myr; and (3) erosion rate or, more precisely, presence or absence of coupled erosion. By coupled erosion we mean erosion/sedimentation whose intensity is tuned to balance the tectonic uplift/subsidence [see *Avouac and Burov*, 1996; *Burov and Cloetingh*, 1997].

A series of experiments were conducted to estimate the respective importance of each parameter at a time. For all cases we used a representative continental extension rate of 25 mm yr^{-1} and initial crustal thickness of 40 km [e.g., *Doser and Yarwood*, 1994]. A three-layered rheological structure (Figure 1c) was imposed: 20 km thick upper crust, 20 km thick lower crust, and 80 km thick mantle lithosphere.

In total, we present the results of 12 experiments (three representative values of age times two values of erosion times two values of synrift duration). Each computer run takes ~ 3-14 days on a biprocessor workstation Sparc Ultra 60 because of high numerical resolution and short computation step needed for localization of shear zones and handling nonlinear rheology. For this reason, there was no possibility to vary parameters at a smaller increment.

Table 1. Basic Parameters Used

Variable/Parameter	Values and Units	Comments
Initial crustal thickness T_c	40×10^3 m	continental crust
Initial upper crustal thickness	20×10^3 m	continental crust
Initial lower crustal thickness	20×10^3 m	continental crust
Extension rate	25×10^{-3} m y^{-1}, 50×10^{-3} m y^{-1}	applied on both sides
Thermotectonic age t_a	50, 250, 400 Myr	young, intermediate, old plate
Coefficient of erosion k	0, 500, 1000 m^2 y^{-1}	zero, intermediate, rapid erosion
Background strain rate $\dot{\varepsilon}$	10^{-17} to 10^{-13} s^{-1}	obtained from calculations
Young's modulus E	80 GPa	all rocks
Poisson's ratio ν	0.25	all rocks
Universal gas constant R	8.314 J (mol K)$^{-1}$	used in power law
Power law constant $A_0 = A_{c1}$*	5×10^{-12} Pa^{-n} s^{-1}	dry quartzite (upper crust)
Power law constant $n=n_{c1}$	3	dry quartzite (upper crust)
Creep activation entalphy $H^*= H^*_{c1}$	190 kJ mol^{-1}	dry quartzite (upper crust)
Power law constant $A_0 = A_{c2}$*	5.01×10^{-15} Pa^{-n} s^{-1}	dry diorite (lower crust)
Power law constant $n=n_{c2}$	2.4	dry diorite (lower crust)
Creep activation entalphy $H^*= H^*_{c2}$	212 kJ mol^{-1}	dry diorite (lower crust)
Power law constant $A_0 = A_m$ *	7×10^{-14} Pa^{-n} s^{-1}	olivine
Power law constant $n=n_m$	3	olivine
Creep activation entalphy $H^*= H^*_m$	520 kJ mol^{-1}	olivine
Density ρ_s	2300 kg m^{-3} at 0°C	uncompacted sediment
Density ρ_{c1}	2650 kg m^{-3} at 0°C	upper crust
Density ρ_{c2}	2900 kg m^{-3} at 0°C	lower crust
Density ρ_m	3330 kg m^{-3} at 0°C	mantle
Gravity constant g	9. 8 m s^{-2}	
Initial thermal thickness of the lithosphere a_t	150×10^3 , 250×10^3 m	corresponds to the depth to 1330°C
Temperature at the Base a_t of the lithosphere T_m	1330°C	used to compute initial geotherms
Thermal diffusivity χ_{c1}	8.3×10^{-7} m^2 s^{-1}	upper crust
Thermal diffusivity χ_{c2}	6.7×10^{-7} m^2 s^{-1}	lower crust
Thermal diffusivity χ_m	8.75×10^{-7} m^2 s^{-1}	mantle lithosphere
Thermal conductivity k_s	1.6 W m^{-1} K^{-1}	uncompacted sediment
Thermal conductivity k_{c1}	2.5 W m^{-1} K^{-1}	upper crust
Thermal conductivity k_{c2}	2 W m^{-1} K^{-1}	lower crust
Thermal conductivity k_m	3.5 W m^{-1} K^{-1}	mantle lithosphere
Radiogenic decay depth h_r	10×10^3 m	upper crust
Surface heat production H_s	9.5×10^{-10} W kg^{-1}	upper crust
Coefficient of thermal expansion α	3.1×10^{-5} K^{-1}	
Coefficient of erosion k	200–1000 m^2 y^{-1}	surface processes

The first variable model parameter, thermotectonic age, controls the initial thickness of the competent and ductile rheological layers and thus predefines three end-member lithospheric structures. By varying this major parameter we simultaneously vary respective thicknesses of the competent and ductile upper, lower crust and mantle lithosphere (Figure 1c):

Structure 1 is young lithosphere with strong crust and weak mantle. This case corresponds to a young hot lithosphere with thermotectonic age t_a =50 Ma (see rheological envelope in Figure 1c). At 50 Ma the mantle layer is almost completely ductile, and its strength is practically negligible. The crust thus dominates in the mechanical response of the lithosphere.

Structure 2 is middle aged lithosphere with strong crust and equally strong mantle (t_a =250 Ma, Figure 1c). This is a geodynamically most important scenario for it likely corresponds to majority of continental rift systems [e.g., *Bertotti et al.*, 2000]. In this case the ductile lower and intermediate crust can form flow channels delimited by rigid flexible crustal and mantle layers, resulting in large diversity of possible mechanical behaviors.

Structure 3 is old lithosphere with strong crust and very strong mantle (t_a =400 Ma, Figure 1c). For thermotectonic ages of 400 Ma and more, the strong mantle layer dominates in the mechanical response of the lithosphere (e.g., Baikal rift [*Déverchere et al.*, 1991; *Doser and Yarwood*, 1994; *Petit et al.*, 1997]).

Plates 1 and 2 and Figures 2 and 3 will show direct results of the numerical experiments (shear stress, velocity, temperature or strain rate fields), whereas Figure 5 will present the geodynamic structural interpretation of these experiments. Reading numerical results requires some experience, and we note that the shear stress patterns are useful to estimate the current integrated strength of each individual rheological layer, which is roughly proportional to the thickness of the respective high stress zone multiplied by the normalized average stress value in it. More quantitative integrated strength estimates will be given in Figure 4. Localized strain rate patterns

indicate shear zones, such as zones of active faulting or of decoupling between the rheological layers or zones of intensive ductile flow.

3.1. Structure 1 (Young Age, t_a = 50 Ma): Strong Upper Crustal Layer and Weak Underlying Layers

For t_a=50 Ma, plate strength is concentrated in the upper crust, and the level of necking is very shallow (Figure 1c). The mantle lithosphere thus can be replaced with isostatic thermal basement (Winkler forces plus thermal boundary condition at the bottom), which allows us to reduce the vertical size of the numerical box. Plate 1 presents results of two experiments for a short rifting episode (1.5 Myr). In the case on the left, there is no synrift erosion, and the predicted topography and distribution of faulted blocks closely resemble those observed in the slow spreading oceanic rift zones (numerically reproduced by *Buck and Poliakov* [1998] for oceanic thermorheological settings). This similarity serves as an important test for the model: At the sea bottom, there is little erosion, and it is natural to obtain oceanic basement structures. The case of fast synrift erosion on the right of the Plate 1 is very different. First, though not surprising, the overall form is much smoother, but with shorter length-scale fault blocks well represented. Second, less expected, the thickness and the deep structure of the rift significantly differ from the "oceanic" case shown on the left: extension with coeval erosion results in almost 2 times thinner crust and ~1.5 times larger rift basin. The amount of tectonic stretching is exactly the same in the both cases, but the value of apparent β factor, if one tries to derive it by matching subsidence curves with commonly inferred analytical models [*McKenzie*, 1978], would be ~2 times larger in the second case. In practice, this also means that when seismic or gravity data allow for estimates of crustal thinning (β coefficient) but interpretable stratigraphy data are unavailable (e.g., *Ebinger et al.* [1989] or *Petit et al.* [1997]), attempts to reproduce subsidence history using "observed" β coefficient and the *McKenzie* [1978] model will yield improper reconstruction of synphase thinning, subsidence, and thermal history.

The demonstrated effect of synrift erosion is explained in Figure 1a: Erosion destroys and unloads the uppermost cold and strong crustal layer, which provokes isostatic uplift of weaker ductile crustal material that replaces the strong layer; this replacement locally reduces resistance to tensional stress and results in faster thinning. Synrift depositional load also results in flexure of the plastoductile crust, which provokes localized yielding and weakening in the center of the basin (Figure 1c, see also *Burov and Cloetingh* [1997]), the latter locally reduces resistance to tensional stress and thus accelerates thinning. Long rifting episode (7 Myr) is not shown for the 50 Ma case, because the young lithosphere is so weak that even half of this time (3.5 Myr) is largely enough for initiation of continental breakup, a topic which is beyond the scope of this study.

3.2. Structure 2 (Intermediate Age, t_a = 250 Ma): Equally Strong Crust and Mantle Layers

This initial structure is representative for the majority of rift systems with initial thermal age between 100 and 350 Ma.

3.2.1. Early extensional phase. In this case (Figures 1c and 2), there are initially three competent layers of comparable thickness (the upper and lower crustal and mantle one) mechanically decoupled from each other by low strength ductile layers resulting from differences in creep activation temperatures specific for respective lithologies (Table 1). As expected [*Burov and Cloetingh*, 1997], such decoupling results in very weak behavior of the rift because the flexural resistance (EET) of a decoupled layered system is ~2-3 times smaller than that of a coupled one [*Burov and Diament*, 1995]. In the experiment, viscous and plastic necking occurs independently at different levels in the crust and mantle. Hence the location of the maximum strain zone jumps from one level to another, result-

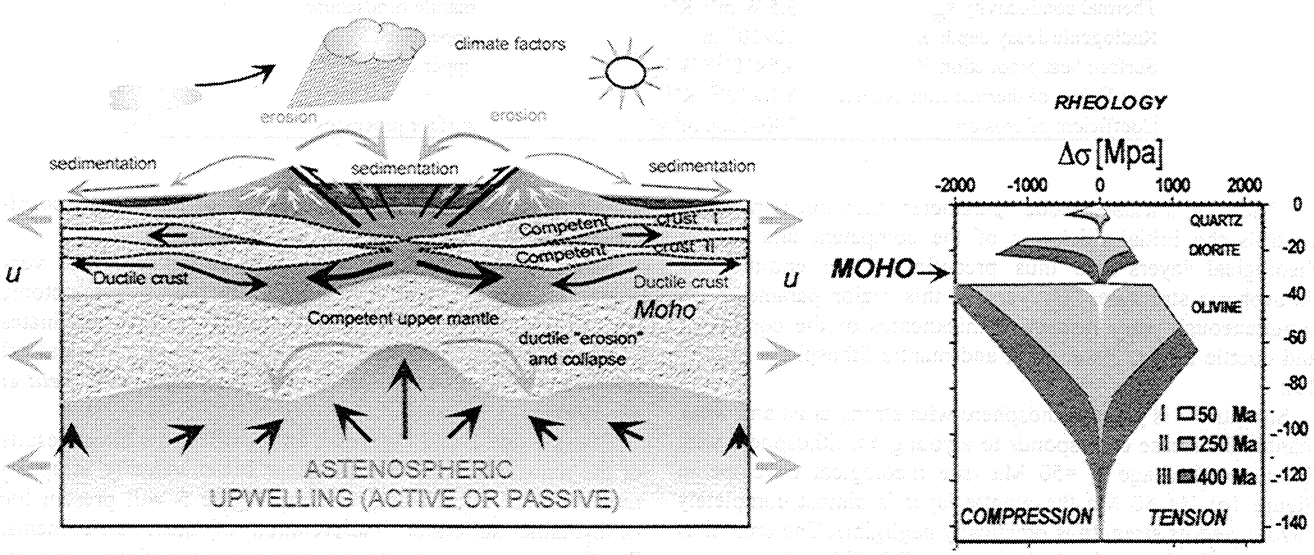

Figure 1c. Sketch of the numerical problem. The sedimentary load derived from erosion on the flanks is accumulated in the basin. Strong parts of the crust and of mantle lithosphere bend under this growing load and weaken due to flexural yielding. As result, the integrated strength is reduced beneath the basin and shoulders (bottom) and with time may become lower than immediately after extension. The lower crustal material flows from center of basin toward the shoulders facilitating their uplift. Two major rheological scenarios are possible: weak lower crust (Figure 1b) and strong basic lower crust (this figure).

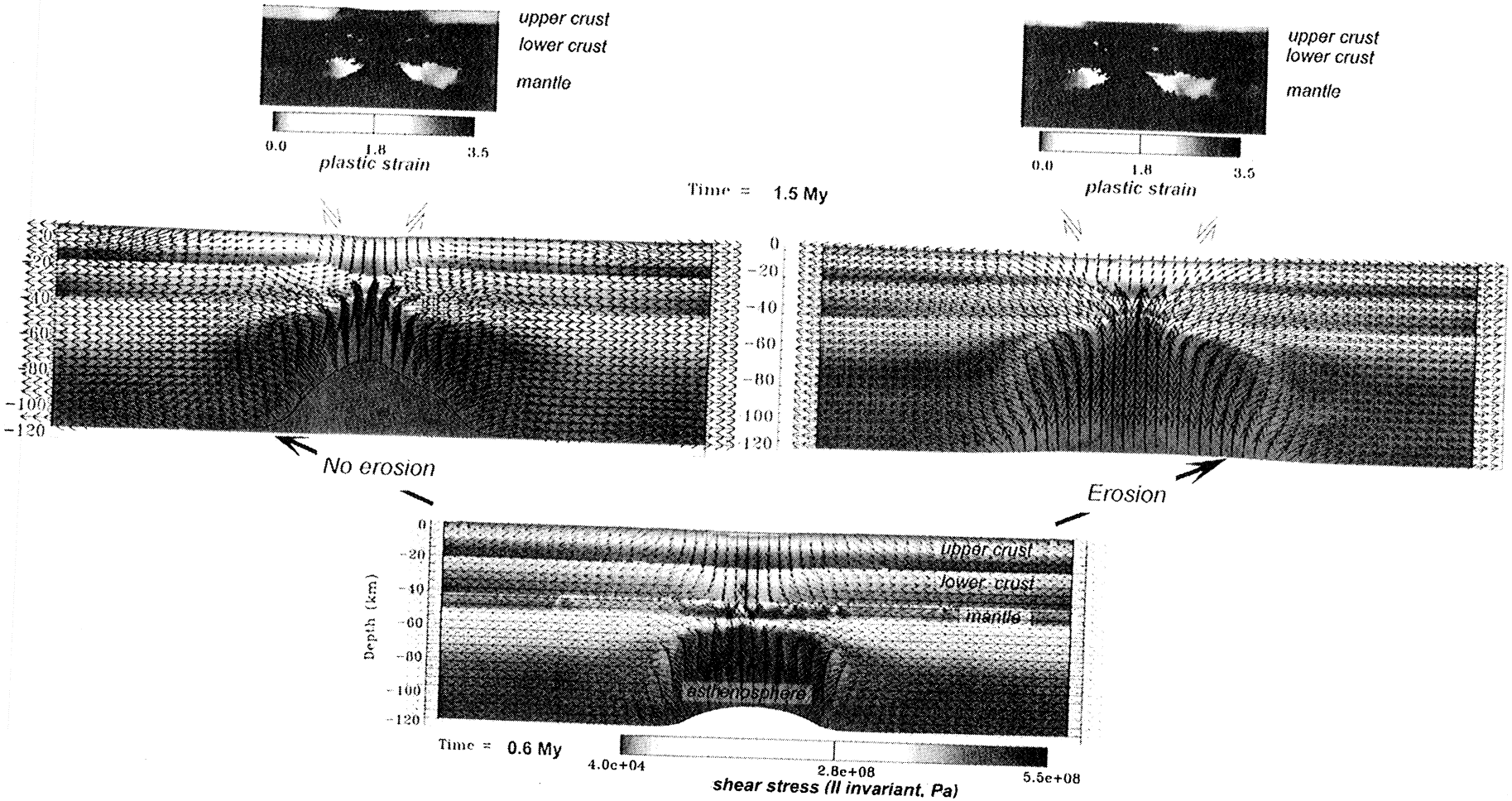

Figure 2a. Numerical model of synrift extension and erosion of a middle-aged multi-layered lithosphere (250 Ma) with competent middle crustal and mantle layers. Note subsidence and uplift periods caused by interplay between sedimentary loading and mechanical response. The degree of strength of an individual rheological layer can be estimated from respective thickness of a high stress zone (see also Figure 3); more quantitative estimations will be given in Figure 4. Experiments are (left) without erosion and (right) with coupled erosion (k=500 m^2 y^{-1}), initial and developed stage of the synrift phase (shear stress and velocity vectors). For the developed stage, accumulated plastic strain (× 100%) in the central part of the rift is shown in the top insert.

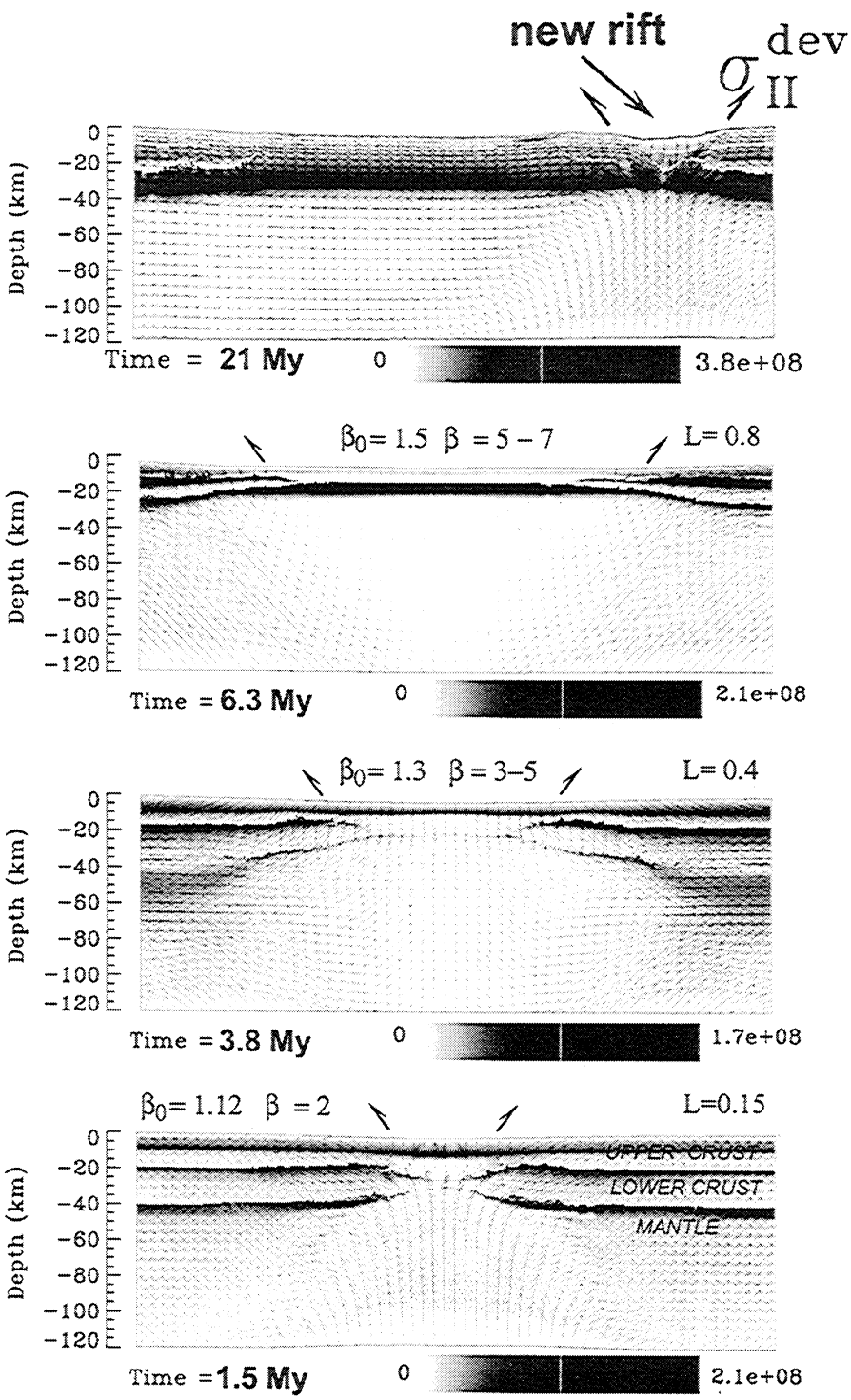

Figure 2b. Experiments with intermediate erosion (k=500 m^2 y^{-1}), consequent phases of synrift evolution (time from 0 to 6.4 Ma) and beginning of the postrift phase (from t > 6.4 Ma). The parameter β_0 is the total extension of the area with respect to the initial model length, β is the resulting apparent stretching factor in the center of the rift, and L is the ratio of the maximum length of the locally thinned area (crust, mantle, and surface) to the initial model length.

ing in strong variations in geometry of the flexural basin and of subsidence rate. The experiment shows that erosion and sedimentation during the synrift stage may invert the direction of the vertical crustal movement (Figures 2a and 2b). Rapid erosional unloading on the flanks and induced ductile crustal flow causes a temporal uplift (duration of ~0.3 Myr in this particular case) in the middle of the basin followed by a slow subsidence. The crustal flow also allows for relative uplift and subsidence of the upper crustal, lower crustal and, mantle parts. Comparison of the experiments with zero and strong

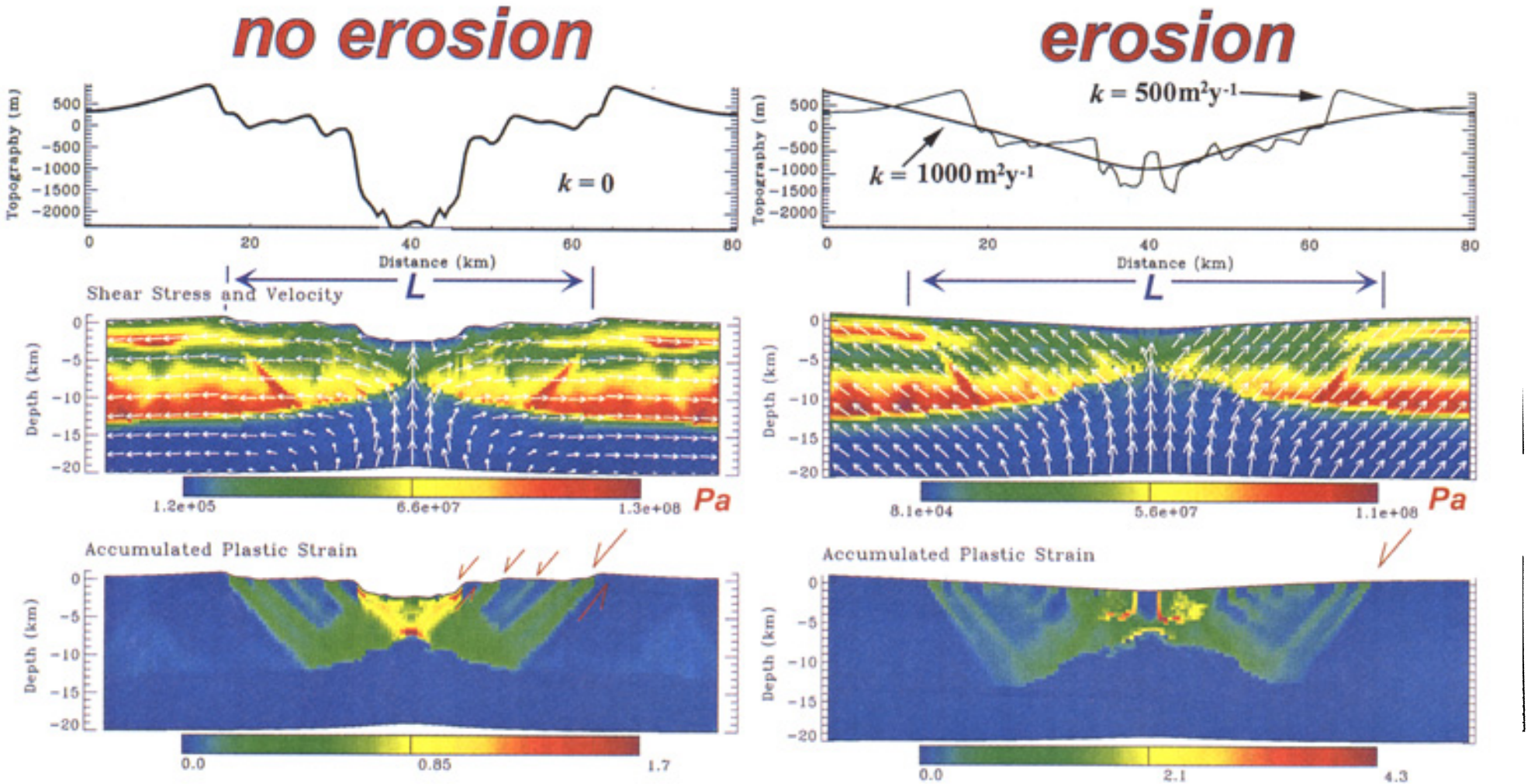

Plate 1. Numerical model of synrift extension of a young lithosphere (age 50 Ma, extension rate 25 mm y^{-1} at both sides): (top) computed surface topography; (middle) shear stress and velocity vectors and (bottom) accumulated plastic strain. The experiments shown on the left- and right-hand sides are identical except that on the left there is no erosion, whereas in the case shown on the right, there is rapid erosion (coefficient of erosion k=1000 $m^2 y^{-1}$). On the right, surface topography for intermediate k=500 $m^2 y^{-1}$ is also shown. Erosion results in stronger thinning of the rift and produces a larger basin.

synrift erosion (Figure 2a) allows us to conclude that coupled surface processes not only accelerate or retard extension (as in the case of Plate 1) but also influence the level of necking, resulting in strongly different basin geometries and different synrift and postrift subsidence histories.

3.2.2. Late extensional weakening. At later stages of the synrift phase the crustal and mantle rigid cores vanish and disappear in the middle of the rift, where the strong material from the ruptured competent layers is replaced by weak ductile material. Rupture of the strong lower or intermediate crustal core results in abrupt reduction of the mechanical resistance to the ascent of the hot mantle/asthenosphere. The latter ascends, producing accelerated Moho uplift, whereas the ductile upper crust fills in the space previously occupied by the lower crust, resulting in accelerated basement subsidence. Late stage extension (Figure 2b) results in complete rupture of all competent layers. Ruptures of the layers are not simultaneous (unless by coincidence) and are followed by abrupt weakening of the system and consequent vertical acceleration of the lithospheric layers (Figures 2a and 2b).

3.2.3. Late extensional strengthening. The same amount of extension results in abrupt strengthening of the rift if the competent layers get close together before the final rupture. Indeed, thinning results in the decrease of the distance between the competent layers, which forces the ductile crust to squeeze out laterally toward the rift shoulders (Figure 2). When the strong cores of the upper, lower crustal, and mantle layers join each other, they become mechanically "welded" (Figure 2b), or coupled, and the flexural strength of the lithosphere (EET) should double or triple (section 2.4). This strength increase arrives well before the lithosphere starts to strengthen by cooling. Welded crustal layers form a single necking zone. The welded mantle/asthenosphere multilayer approaches the surface, cools, and becomes even more strong. Outward expulsion of the ductile material, provoked by interlayer "welding" in the middle, contributes to the uplift on the rift flanks and crustal thickening outside of the basin, as has been interpreted in several seismic studies of active rift zones [e.g., *Ebinger et al.*, 1999]. The basin subsidence slows down and is followed by lateral enlargement of the basin. As can be seen from Figure 2, welding of the competent layers in the middle of the basin is preceded by similar welding under the rift flanks, which locally doubles the elastic thickness in the flank area. Bending stress tends to zero in this area, and thus inelastic flexural weakening is also lowest here (see also Figure 1b). Such localized flexural strengthening at rift borders helps to maintain the flank uplift. It is noteworthy that gravity and apatite fission track studies of, for example, the rift flanks of the East African Rift system, confirm that the extended continental lithosphere maintains considerable strength during the synrift stage, leading to long-lived rift flank uplift [*Karner and Watts*, 1982; *Bechtel et al.*, 1990; *Ebinger et al.*, 1989;1991, 1999; *Ebinger and Sleep*, 1998].

3.2.4. Late extensional complexities. Depending on which event occurs earlier, rupture of the competent layers or their mechanical coupling, basin subsidence sharply accelerates or slows down. One of the layers can be deflected more than others, creating a relative depression (or relative thickening) in the ductile crust under the basin. This depression drives inflow of the ductile crust from outside of the basin and results in retardation (even in relative uplift) or acceleration of basement subsidence. As suggested by *Royden and Keen* [1980], *White and McKenzie* [1988], and *Kaufman and Royden* [1994], the averaged crust and mantle β factors may differ within a basin. Our experiment suggests that the internal crustal levels may also exhibit different β factors and even be deflected in opposite directions. For example, the upper crustal layer may subside while the lower or intermediate crustal layers move upward (Figure 2).

3.2.5. Postrift phase. In addition to the semianalytical results of *Burov and Cloetingh* [1997], who have shown that surface processes and induced crustal flow enhance total basin subsidence, the experiments demonstrate that thermal subsidence of deep mantle layers may have no immediate effect on the near-surface crustal layers. Strong mantle may subside independent of the strong crust (in time and space), whereas the increasing mantle-crust gap is filled by ductile crustal material. The inflow of the ductile crust under the basin results in thinning and coupling of the crustal layers under its flanks.

3.3. Structure 3 (Old Lithosphere, t_a=400 Ma): Mantle Layer Stronger Than the Crustal Layer

In this case, the strong mantle layer is considerably thicker than the strong crustal layers (Figure 3), and the effective viscosity of the lower crust is high enough to prevent crust-mantle decoupling, so that at the beginning, the crustal deformation is coupled with that of the mantle lithosphere. The rift basin is narrower and deeper than in the previous case. If rifting continues for a significant time period (>3 Myr), the strong mantle layer finally ruptures, allowing accelerated asthenospheric ascent (Figure 3b).

Even in this case the importance of the surface processes is nonnegligible depending on the erosion rate: The erosion and sedimentation (Figure 3) can (1) provoke stagnation and even uplift periods during the synrift phase, (2) favor development of asymmetric extension patterns owing to the fundamental property of the erosion to amplify surface velocity anomalies such as sliding on the faults, and (3) result in localization of faulting at the borders of the rift.

4. More Results and Discussion

4.1. Subsidence and Strength Evolution

Figure 4 shows subsidence and integrated strength (EET) evolution curves for the experiments from Figures 2 and 3, compared to pure thermal subsidence curves. In the experiments shown in Figures 3 and 4 (bottom right), ductile flow and strength variations result in pronounced postrift uplift about 10 Myr after the synrift phase. One can also observe synrift and postrift oscillations in the subsidence rate resulting from interplays between differential necking, ductile flow, surface processes, gravity spreading, and asthenospheric upflow. The relative importance of each of these mechanisms is discussed in sections 4.2-4.7, but one can already emphasize the crucial influence of the surface processes on the mechanical strength of the lithosphere (strong EET reduction) and thus on the overall isostatic response of the rift system (Figure 4b).

4.2. Evolution of the Surface Topography and Crustal Structures

The fully coupled numerical model predicts geologically realistic [e.g., *Salveson*, 1978; *Cloetingh et al.*, 1982; *Buck*, 1991; *Ziegler*, 1994; *Olsen*, 1995] rift and fault structures and stages of rift evolution [*Salveson*, 1978] (Plate 2): Half-graben, graben, continental extensional basin, continental

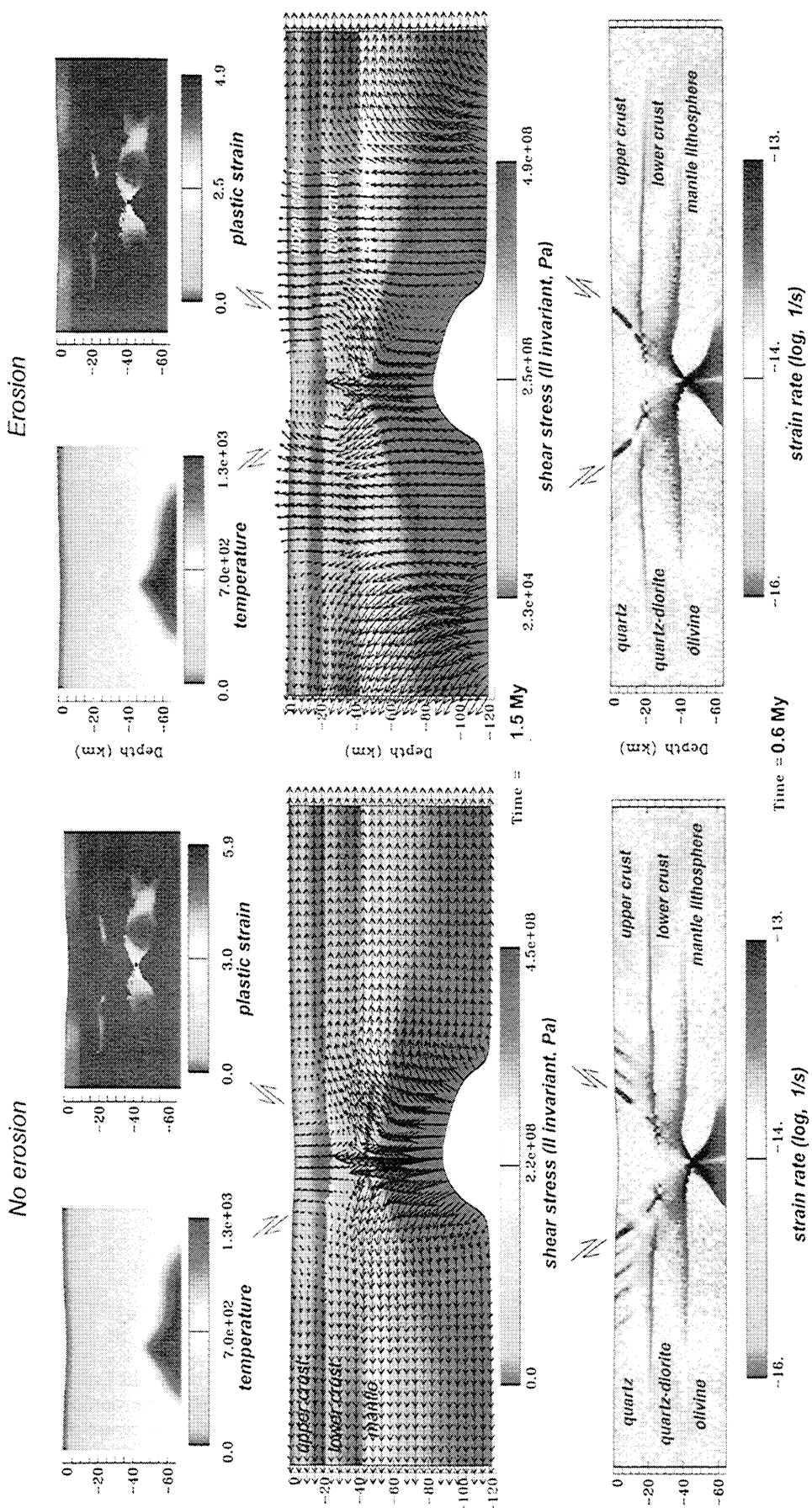

Figure 3a. Extension of old (400 Ma) multilayered lithosphere. Experiments are (left) without and (right) with coupled erosion (k=500 m^2 y^{-1}); initial phase (strain rate, t =0.6 Ma) and developed (shear stress) phase of synrift evolution (t =1.5 Ma). Temperature and plastic strain distributions in the central part of the rift for the developed phase (t =1.5 My) are shown in the inserts.

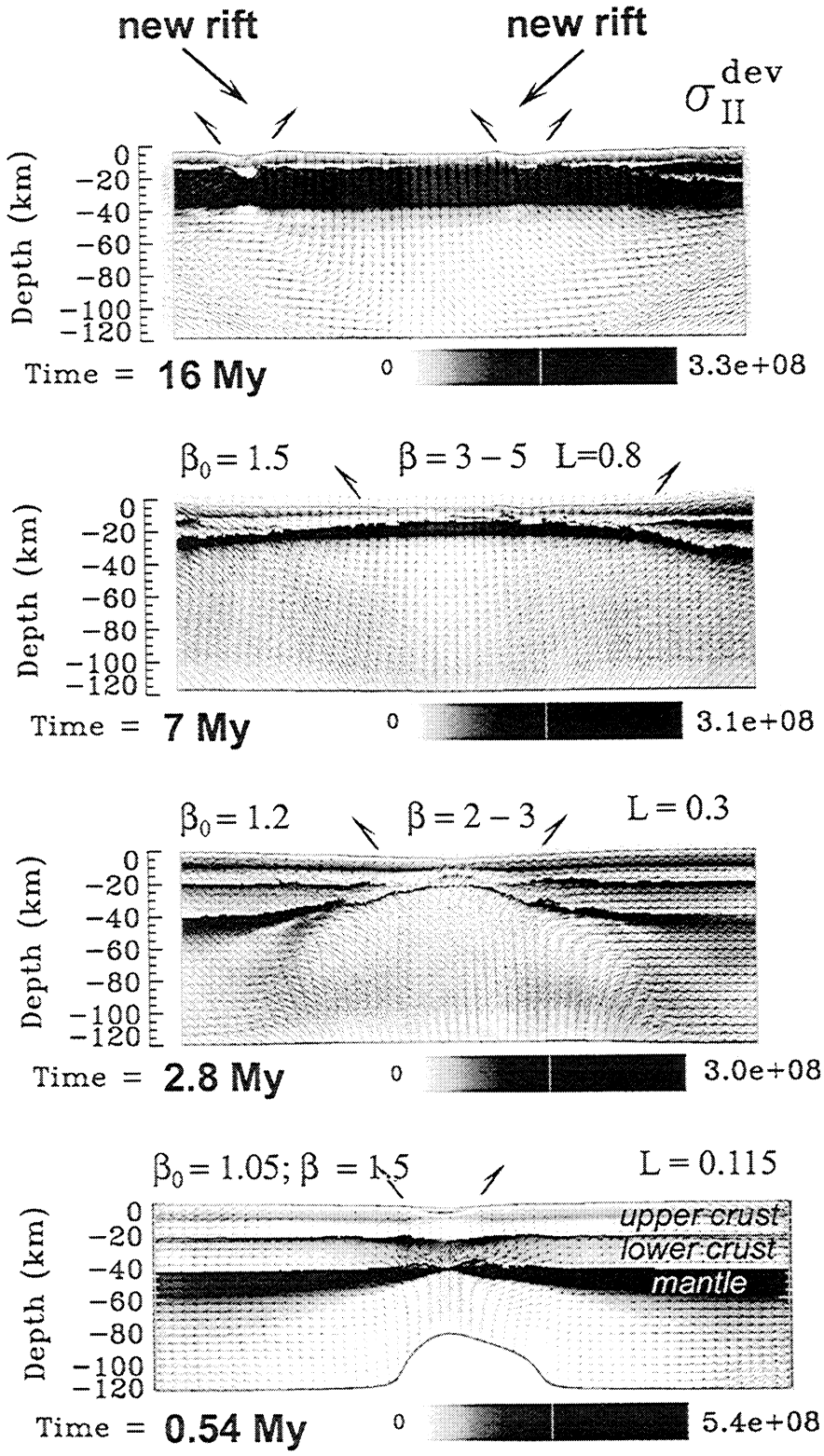

Figure 3b. Experiments with intermediate erosion (k=500 m^2 y^{-1}), consequent phases of synrift evolution (0-6.4 Ma) and beginning of the postrift phase (t > 6.4 Ma). The parameter β_0 is the total extension of the area with respect to the initial model length, β is the resulting apparent stretching factor in the centre of the rift, and L is the ratio of the maximum length of the locally thinned area (crust, mantle, and surface) to the initial model length.

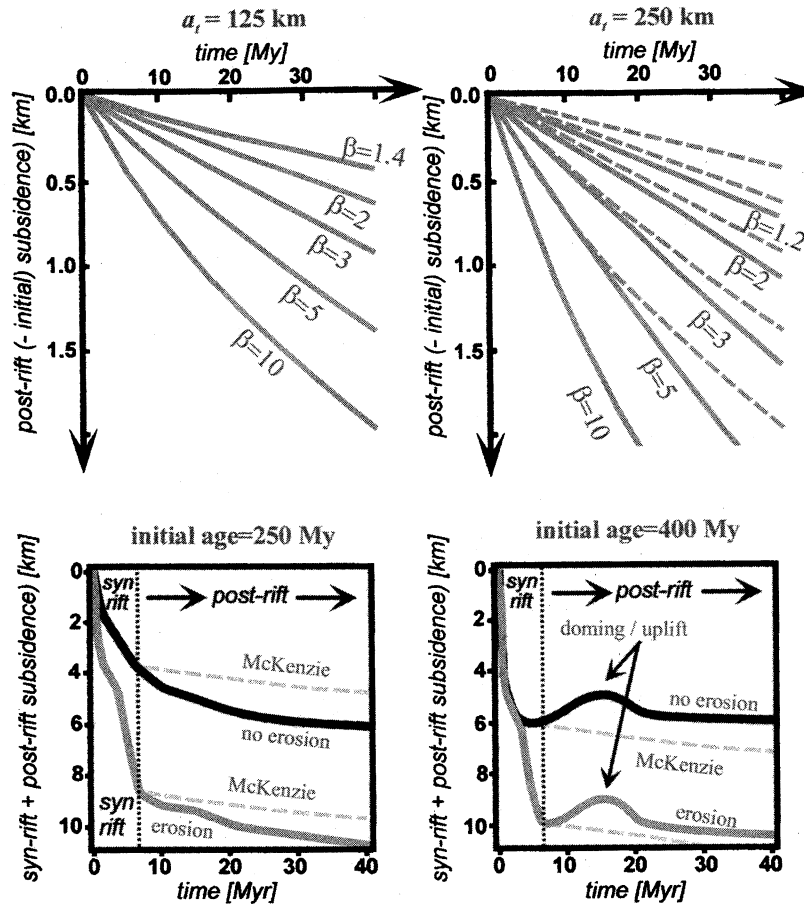

Figure 4a. Strength evolution in the center of the rift and subsidence stages produced by the numerical experiments from Figures 2 and 3 compared to common thermal subsidence model. Thermal subsidence is shown by curves for the commonly used *McKenzie* [1978] model predicting subsidence after extension ceased, (top left) those for a_i=125 km (a_i is the initial depth to isotherm 1330°C, called thermal thickness of the lithosphere), (top right) analogous curves for a_i=250 km (solid lines) compared with a_i=125 km (dashed line), (bottom) subsidence curves produced by the model (with and without erosion), (bottom left) subsidence curves for thermotectonic age 250 Ma (a_i=250 km), and (bottom right) subsidence curves for thermotectonic age 400 Ma (a_i=250 km). Shaded dashed lines show predictions of the respective McKenzie models.

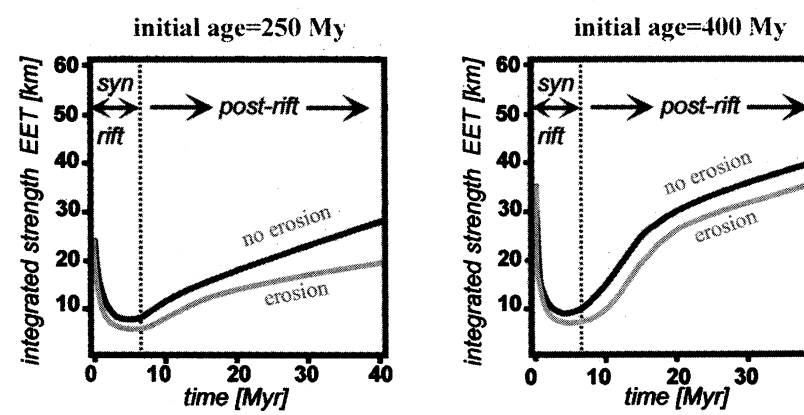

Figure 4b. Integrated strength evolution expressed in terms of EET (equivalent elastic thickness). (left) EET evolution for initial thermotectonic age of 250 Ma. (right) EET evolution for initial thermotectonic age of 400 Ma. Note that rapid increase in EET on the postrift phase is related to extension-induced replacement of the weak crust by mantle/asthenosphere material, which rapidly becomes strong with cooling.

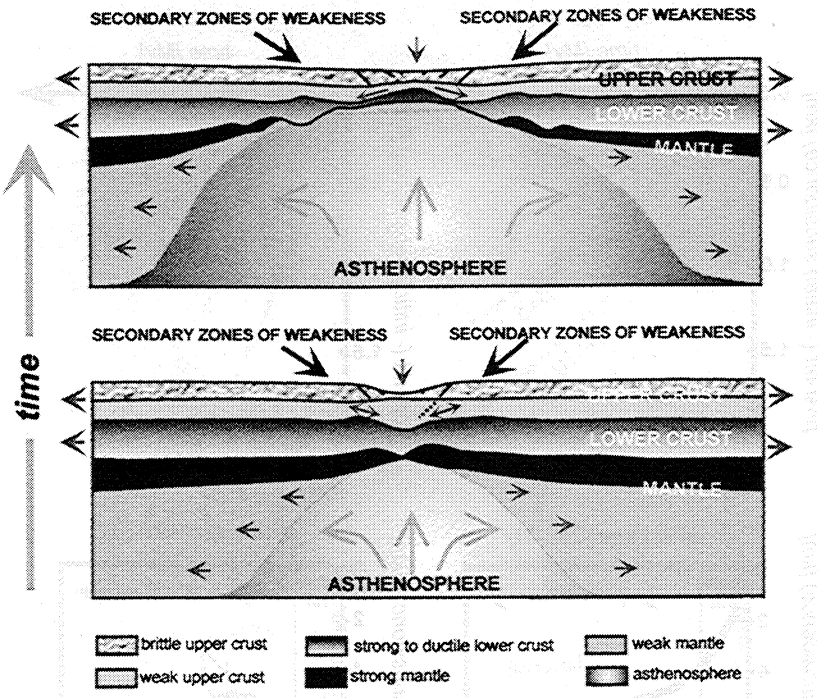

Figure 5a. Structural and geodynamic interpretation of the numerical experiments for main stages of synrift evolution of a rift with relatively "hot" (weak) structure.

breakup, and narrow and diffuse rifting. The response of a young lithosphere is controlled by a single competent layer, and thus the overall behavior is similar to that of the oceanic spreading zones (Plate 1), already discussed, for example, by *Buck and Poliakov* [1998]. Synthesis of the experiments on the behavior of older lithosphere is presented in Figure 5. The following phases are predicted.

4.3. Intermediate Themotectonic Age (Structure 2)

1. The deformation in Figure 5a is first concentrated in the deepest thin competent mantle layer, resulting in a rapid subsidence. This layer is soon disrupted in the middle, and the extension switches to the shallower lower crustal layer. In spite of that, the boundary conditions correspond to passive rifting; the induced uplift of hot asthenosphere seemingly plays a major role in the extension of the bottom layers due to their strong strain rate and temperature sensitivity.

2. The space in the middle previously occupied in phase 1 by ruptured strong mantle layer is filled with ductile crustal material from above and with weak mantle/asthenospheric material from below. The outflow of the ductile crustal material to the center of the basin temporally accelerates surface subsidence. If subsidence is followed by fast synrift sedimentation, this outflow results in outward lateral spreading of the ductile upper crust, which provokes further acceleration of surface subsidence.

3. If rifting continues after phase 2, the strong lower crustal level also becomes ruptured, both as a result of accelerated thermal weakening by direct heating from the ascending asthenosphere and as a result of flexural yielding. The space previously occupied by strong lower/intermediate crustal layer is filled with ductile upper crustal material, which spreads down to the lower crustal depth until direct contact with the uplifted hot mantle/asthenosphere. This contact has crucial consequences because the viscosity of this quartz-rich material is hypersensitive to heat, so that the upper crustal layer rapidly weakens, resulting in its accelerated lateral spreading and surface subsidence. Partial melting in the upwelling asthenosphere and intrusion of melts in the crust (not accounted for in this study) may also result in additional weakening of the overlying crust.

4. In the long term, extension leads to "overstrengthening" of the lithosphere, which is additional strengthening compared to the "normal strengthening" due to cooling first discussed by *England* [1983] and *Dunbar and Sawyer* [1988]. This overstrengthening is associated with structural and rheological changes provoked by thinning. As was quantitatively shown by *Burov and Diament* [1995], for a simple steady state geotherm the thinner the crust, the stronger the lithosphere. Indeed, when the mantle/asthenosphere layer approaches the surface, it rapidly cools and strengthens due to the steep near-surface geothermal gradient [e.g., *England,* 1983]. This results in gradual strength recovery of the mantle/asthenosphere layer beneath the extended upper crust. If mechanical coupling of this layer with the crust occurs, the coupling leads to dramatic increase of the flexural resistance of the system, and consequently in the abrupt retardation of the thermal subsidence. Because of nonlinear sensitivity of the mantle to the temperature variations, on the postrift stage the flexural strength recovers and grows faster than the rate at which thermal distribution returns to the pre-rift steady state. Crustal material is already weak at 300°C, whereas the mantle/asthenospheric material is much more resistant and needs to reach 700-800°C for creep activation. Mantle/asthenosphere uplifted to the crustal depth cools below 700°C and becomes far stronger than the crust. Consequently, the flexural strength of the system in the center of the basin becomes higher than that before extension

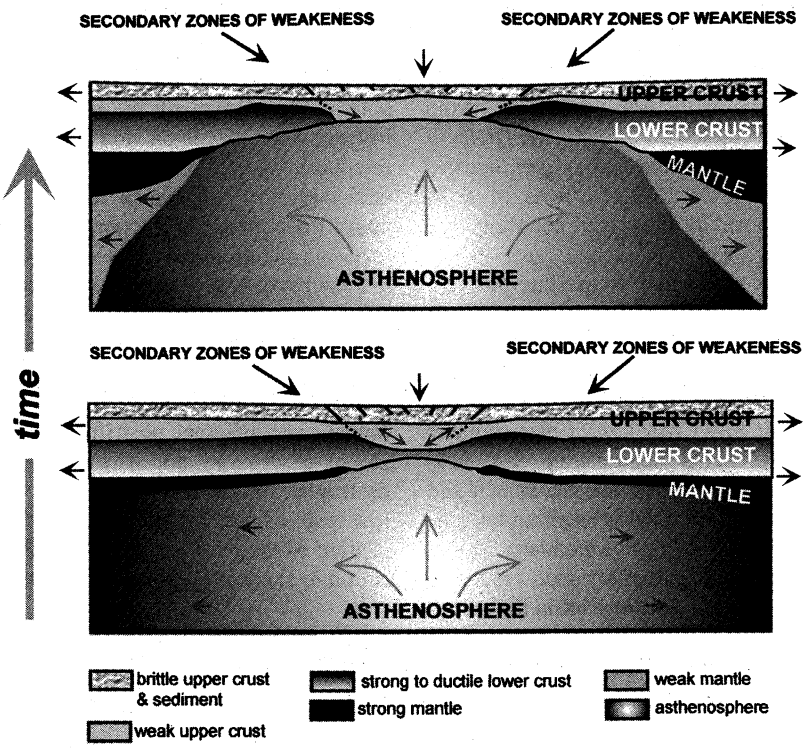

Figure 5b. Main stages of synrift evolution of a rift with initially "cold" (strong) structure.

(Figure 4b). It also becomes higher than that just outside the borders, which correspond to the predicted secondary zones of flexural weakening (Figures 1b and 1c). It is thus the border areas that become new zones of potential rifting, providing a mechanism for the lateral migration of rifts [e.g., *Ebinger et al.*, 1999]

For example, in the case shown in Figure 2 the initial EET of the lithosphere is roughly equal to h_m (t=0) - EET_c (t=0) ≈ 25 km, where h_m is the depth of mantle creep activation, which corresponds to the isotherm 700-800°C (h_m ≈65-70 km for 250 Myr old lithosphere), and EET_c is the thickness of the competent crustal layer only. With β=4, 50 Myr after extension the isotherm 700-800°C is found at 40-45 km depth and T_c (t=50 Ma) ≈ 1/4 T_c (t=0). At pressures corresponding to the 40 km depth the mantle rocks flow at 600°C, which yields h_m ≈ 35-40 km and EET values (h_m (t=50 Ma) - T_c (t=50 Ma)) of about the initial value of 25 km. At 100 Ma, EET beneath the basin will be about twice the preextensional value, which is ~1.5 times higher than the upper bounds on "normal" EET increase due to cooling with age [*Burov and Diament*, 1995].

5. For the postrift phase evolution the two-dimensional (2D) experiments confirm the analytical 1½ D results by *Burov and Cloetingh* [1997] (Figures 1b and 1c). These results were derived using a small strain thin layer model, which applied equivalent normal stresses to simulate erosion/sedimentation and did not account for the intermediate crust, faulting, and asthenospheric flow. Our new large-strain 2 D experiments confirmed that in the case of strong postrift sedimentation the basement may flex down at a rate exceeding the thermal subsidence rate, so that the incoming surface load

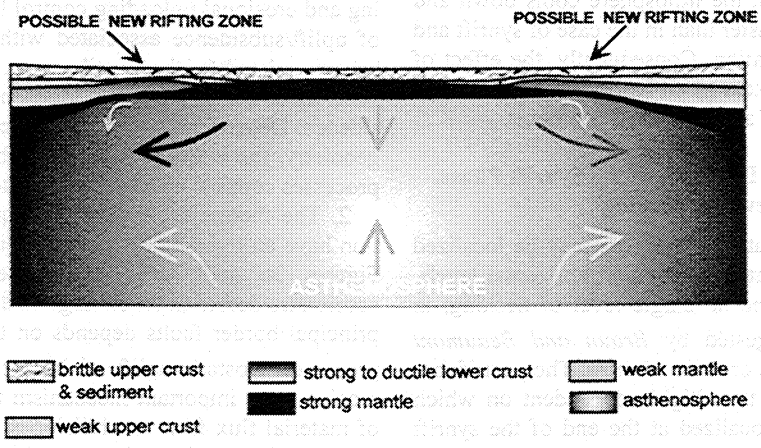

Figure 5c. Postrift evolution of a large basin (strong extension).

is compensated in the ductile crust. Sedimentary load is a thermal insolator, and it retards cooling of the lithosphere beneath the basin [e.g., *Stephenson et al.,* 1989]. In our model, sedimentary loading also results in flexural weakening of the underlying layers, an effect predicted by *Burov and Diament* [1992], *Burov and Cloetingh* [1997], and *Lavier and Steckler* [1997] (Figure 1b). The thermomechanical effects of sedimentation are opposite to those of interlayer coupling and strengthening due to cooling. The subsidence rates in the postrift stage are thus strongly controlled by the interplay between the mechanical strength of the basin and accumulation of the sedimentary load. In all cases the lithosphere is flexurally weakened not only beneath the center of the basin but also immediately outside of the rift flanks, confirming the small strain models *of Burov and Cloetingh* [1997] (Figures 1b and 1c). The new experiments demonstrate that with strengthening of the center of the basin on the late synrift and early postrift stages, these external areas of weakening become possible candidates for localization of secondary rifting zone(s). The accumulation of the sedimentary load results in lateral spreading (Figures 2b, 3b, and 5) of the basin and, naturally, in additional superficial extension. Postrift extension can be driven by lateral flow in the ductile crust and by asthenospheric flow induced partly by gravity spreading and partly by the development of a convective instability in the asthenosphere [e.g., *Fleitout and Froidevaux*, 1982; *Huismans et al.*, 2001], allowing the creation of secondary rifting zones without any far-field extension. Such secondary or diffuse rifting zones were not reproduced in the previous studies. Instead, lateral migration or broadening of rift zones had been attributed solely to flexural rotation of faults to angles unfavorable to extension [e.g., *Buck*, 1991; *Forsyth*, 1992].

4.4. Strong Cold Lithosphere (Structure 3)

The evolution of old and cold lithosphere (Figure 5b) demonstrates mostly the same effects as obtained for the intermediate aged lithosphere in section 4.2. The major difference is that the deformation starts from the mantle layer but then is rapidly distributed between the lower crustal and mantle layer. The resulting basin is narrow. The complete rupture of the lower crustal layer is less likely than in the previous younger case. Yet this depends on the duration of rifting and lower crustal rheology, both of which may vary at important extent. The flow in the ductile upper crust is limited to shallower levels. In the case of no important synrift erosion and long extension (Figure 4a,b), the lithosphere cools down and strengthens ~1.2-1.5 times faster than in the case of synrift and immediate postrift sedimentation. Consequently, the effect of sedimentation (thermal blanketing) on late stages of extension is partly equivalent to that of a hotter initial geotherm.

4.5. Polyphase Subsidence, Duration of the Synrift Phase, Subsidence History, and Level of Necking

Figures 2 and 3 show that the extension may be localized simultaneously or consequently on different horizontal levels. For this reason, there will be no single level of necking, in contrast to what was suggested by *Braun and Beaumont* [1989], but there will be two or three of them. The postrift behavior of the rift system is thus highly dependent on which level(s) the extension was localized at the end of the synrift phase. In nature the duration of this phase may vary for it is controlled by external factors, especially in the case of passive rifting. In the experiments shown in Figures 2 to 5 the synrift phase was quite long (7 Myr). As can be seen, by the end of this period the rift structure does not change any more, and the postrift subsidence will follow more or less the same scenario. In turn, if the extension stops earlier at 1, 2, or 3 Myr, the difference in the following postrift behavior will be crucial. In this case, the subsidence history and response to possible postrift compression or extension depends on which structural level(s) (mantle or lower or upper crust or two or all of them) the extension was localized at the end of rifting. This level depends not only on the amount of extension but also on its rate, which controls both the rheological response and synrift heat exchanges. Consequently, for equivalent initial thermo-mechanical structures and amounts of synrift extension, one can obtain very different postrift subsidence histories. For example, extension may stop when the strong mantle level is not yet destroyed. In this case the system will behave as a rift with a low level of necking. In turn, if extension terminates after the rupture of the mantle level, the following behavior will correspond to shallow or intermediate level of necking.

4.6. Postrift Uplift and Delayed Subsidence

1. Similar to predictions made in a number of past and ongoing studies [*Buck*, 1986; *Huismans et al.,* 2001; R.S. Huismans and Y.Y. Podladchikov, Necking and finite amplitude convective instability of the lithosphere, submitted to *Geophysicical Research Letters*, 2000], our model shows that the extension may provoke an instability in the advected asthenosphere, which first starts to ascend in a passive mode but then can continue upwelling in the active mode. This ascent results in supplementary extension (transition from passive to active rifting) followed by retarded postrift uplift or doming which occurs several million years after the synrift phase. Indeed, such uplift is well represented in the experiments on the "old" lithosphere (Plate 2, bottom right).

2. The other reason for delayed postrift subsidence or uplift is inward ductile crustal flow resulting from postrift gravity collapse of the rift flanks. This effect will be important only for relatively narrow basins.

3. Postrift subsidence can be also retarded in a result of formation of strong mantle-asthenosphere layer and its coupling with the crust.

4.7. Influence of Erosion

1. The 2 D experiments confirm that the sedimentary loading and erosional unloading control lateral crustal flow. A part of uplift/subsidence associated with surface loading may be accommodated in the ductile crust. In this case the surface subsidence occurs relatively independently of the mantle subsidence. Dependent on the rheological state and initial crustal geometry, the interaction between the surface and subsurface processes controls up to 50% of the total subsidence.

2. The thermomechanical consequences of the sedimentation have an overall impact on the lithospheric behavior (e.g., Figures 3b and 3c): Erosion effectively localizes and accelerates deformation on large faults so that formation of the principal border faults depends on the activity of the surface processes. Isostatic uplift of the rift shoulders in response to erosion is an important mechanism that maintains a high rate of material flux from the hillslopes. However, erosion on the drainage divides formed by the rift flanks results in their retreat from the center of the basin even without concurrent tec-

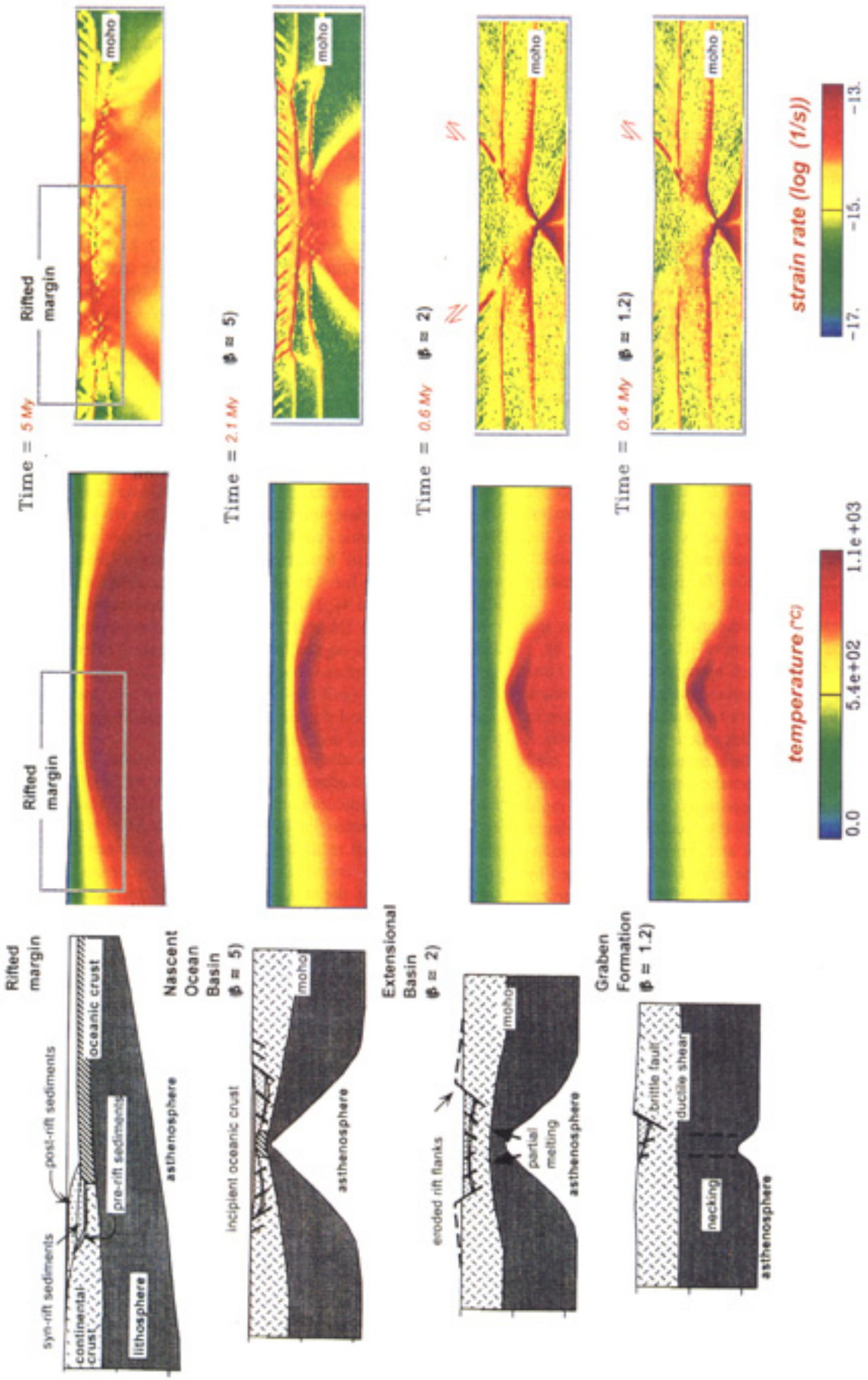

Plate 2. Comparison of various rift structures and fault distributions derived from observations as a function of (left) the coefficient of extension (adopted from *Salvenson* [1978]), with the internal and fault structures produced by the numerical experiments (thermotectonic age of 250 Ma), (middle) temperature field, and (right) strain rate field. Note the strongly two-dimensional character of the temperature field and sharp narrow thermal localization at the top at earlier stages of rift evolution (resulting from nonlinear rheology).

tonic extension. At the same time, the sedimentary wedge migrates toward the center of the basin [e.g., *van Balen et al.*, 1995] (Figure 4 and Plate 2). Such migration of the sedimentary load causes stress variations and characteristic stratigraphic onlap patterns that can be matched with the observations. The geometry of the rift shoulders and stratigraphic patterns are also highly dependent on the assumed erosion law (equations (1-3)).

3. When the erosion (and sedimentation) is slow, the basin is underfilled and, consequently, undercharged, and its subsidence is retarded. The related pressure gradients are insufficient to counteract the pressure gradients due to density contrasts between the crust and mantle beneath the rift shoulders. The net flux in the lower crust can be reversed in this case. It will thus retard the subsidence of the basin and accelerate collapse of the rift shoulders, similar to what was shown by *Burov and Cloetingh* [1997] for the postrift phase only. For narrow rifts with thick ductile crust, this flux may produce a local domal uplift at the end of the synrift/beginning of the postrift phase (see discussion above).

4. Accumulation of the eroded matter requires an adequate increase of the basin volume in time. This can occur both in the vertical and horizontal directions by increase of the depth of the basin due to subsidence or by progressive horizontal spreading and onlap of sedimentary deposits. The result of the latter process is widening of the basin and its "self-extension." This gravity-driven extension is also facilitated by secondary postrift extension due to diverging flow in the lower crust.

5. In nature, erosion cannot respond immediately to the changes in the surface uplift because it is influenced by a number of nontectonic factors, such as regional climate. Time is also needed for the sediments derived on the slopes to reach the basin and for the lower crust to respond to the changes in the surface load. This may introduce delays in the feedback between the surface and subsurface processes that, as well known from the basics of the automatic control theory, results in oscillations in the system, especially in cases of rapid changes in the system input or in the feedback loop. Hence one can predict some extensional and compressional oscillations, as well as oscillations in the subsidence rate caused by temporal disbalances between subsurface and surface processes. Such oscillations in the rate of basin subsidence are reproduced in the numerical experiments and in several natural examples (e.g., Dnieper-Donez basin). Although the latter can be probably explained by eustatic changes, the "feedback" nature is also not excluded.

5. Conclusions

Extension of multilayered lithosphere develops as a sequence of accelerated subsidence phases provoked by nonsimultaneous weakening and ruptures of competent rheological layers separated by weak ductile layers. Synrift basin subsidence results from differential thinning of these layers (this is not a new result) but equally (new quantitatively demonstrated result) from lateral and downward outflow of the ductile crustal material provoked by synrift surface processes and ruptures of the competent layers.

Some results of this study existed previously in the form of qualitative geological ideas, which now find a quantitative validation in a physically consistent model. In this study we demonstrated the following:

1. For typical initial lithospheric structures and apparent coefficients of extension (from 2 to 5), crustal flow coupled with surface processes accelerates synrift subsidence rates by a factor of 1.5-2, increases crustal thinning by a factor of 1.5-2, and preserves uplifted rift shoulders on the time scale of 1 to 50 Myr (Figure 4). Coupling results in variations in the width of the basin during both synrift and postrift phase and drives secondary extension during the postrift phase. Misbalanced surface processes result in the opposite effect: They facilitate collapse of rift shoulders, reduce synrift thinning, accelerate postrift thickening, result in basin uplift, and drive some postrifting compression. Delays (around 0.1 Myr) that may naturally appear in the feedback between the tectonic action (subsidence) and morphologic reaction (surface processes) produce short timescale oscillations in the system (uplifts and sinks without apparent reason).

2. The synrift erosion and sedimentation locally reduce resistance to tensional strain via (1) localized reduction of the thickness of the competent crustal layers and (2) flexural yielding. This leads to amplification of crustal thinning by a factor of 1.5. The role of synrift phase erosion is especially important for young rifts (initial age < 50 Ma) or for those with weak lower crustal rheology (e.g., quartz controlled), where it may increase thinning and width of the rift basin by a factor of 2. Dynamic redistribution of the surface load modifies the strength of the underlying lithosphere (from 100% strength reduction for < 50 Ma lithosphere to 20% for 400 Ma lithosphere, Figure 4). This strength evolution results from the previously known thermal effects [e.g., *Stephenson et al.*, 1989] and in equal degree from inelastic flexural effects (predicted for postrift phase only by *Burov and Cloetingh* [1997]). Flexural yielding significantly modifies synrift and postrift geometry of strong and ductile crustal layers and Moho and particularly the level of necking.

3. In the "coupled erosion and tectonics" mode, synrift and postrift subsidence occurs at rates that differ by 20-50% from those inferred from commonly used models [*McKenzie*, 1978] and can be characterized by long (1 to 10 Myr) periods of stagnation or uplift resulting from interplay between different rheological layers, crustal flow, and surface processes. In particular, rupture of the quasi-elastic core of the intermediate crustal level results in rapid uplift of the mantle layer. Joining (welding) of the rigid lithospheric layers followed by expulsion of the ductile crust results in temporal flexural strengthening, polyphase subsidence, and widening of the basin. On the postrift phase, multiple periods of stagnation result from interplay between the surface processes and the mechanical response of the lithosphere.

4. For continental lithospheres older than 50 Ma and characterized by a three-layered rheological structure (Figure 1c), interactions between various mechanical layers result in different levels of necking for the same initial structure and boundary conditions. During extension the level of necking switches from deep competent layer (mantle, average depth 35-40 km) to the shallower intermediate crust (~25 km) and then to the upper crust (~15 km). Depending on the duration of the extension, initially morphologically and structurally identical basins may start postrift subsidence phase from shallow, intermediate, or low level of necking. Consequently, the traditional definition of the level of necking cannot be used directly to infer initial lithospheric structure or subsidence parameters, especially if one also takes in consideration the effect of necking level dependence on flexural yielding (conclu-

sion 2). This also makes questionable the estimates of the β factor inferred from present-day crustal geometries and backstripping reconstructions. It appears that the entire concept of necking level should be revised to adopt the possibility of its translation from one competent layer to another. This result would mostly apply to small β factors < 3-5. For higher β factors all layers couple together (e.g., late rifting stages shown in Figures 2b and 3b and Plate 2).

5. Previously it was shown [e.g., *England*, 1983; *Dunbar and Sawyer*, 1988] that extension may induce postrift strengthening resulting from cooling and substitution of the thinned crust by stronger (at low temperature) mantle material. This explains late postrift reduction (at 20-50 Myr) of the subsidence rate. Our study shows that for β > 3, strengthening commences much earlier, during the extensional episode (after 2-5 Myr depending on the extension rate). At this moment it is produced by interlayer coupling, not by strengthening due to cooling, because the latter is compensated by thermal [e.g., *Stephenson et al.*, 1989; *Lobkovsky and Kerchman*, 1992; *Lavier and Steckler*, 1997] and flexural weakening effects [*Burov and Cloetingh*, 1997] during at least the first 10-20 Myr after the onset of extension.

6. In contrast to most previous studies [e.g., *England*, 1983; *Dunbar and Sawyer*, 1988], and in confirmation of some qualitative analytical results obtained by *Burov and Cloetingh* [1997], we show that postrift strengthening results in stronger EET values in the middle of the rift basin than immediately outside its flanks. The rift flank areas stay weak because they are permanently locally weakened by flexure (Figures 1b,1c, and 5) and by enhanced conductive and also as convective heat transport in the lithosphere and lithosphere, respectively, beneath the borders of the extended area. If extension continues, these areas nucleate new rifting. This rift initiation is a larger-scale feature than the results of *Lavier et al.* [2000] on short distance normal fault jumping in extending ideal brittle layer. This secondary rifting may not require any new far-field extensional episode because stresses produced by gravity spreading and induced flows in the ductile crust and the asthenosphere are already sufficient. Interplay between strengthening and extension at the end of a long (e.g., > 5 Myr) synrift phase or at the beginning of a postrift phase may explain so-called abandoned rifts.

Two effects demonstrated in this study produce opposite actions at the end of synrift and during the whole postrift phase. The first effect is acceleration of subsidence resulting from: (1) coupling between the surface and subsurface process, (2) flexural weakening due to increasing sedimentary load, (3) retardation of cooling due heat screening by sediments, (4) thinning of the competent crust by the surface erosion. The second effect is retardation of subsidence resulting from replacement of the weak crust by stronger mantle/asthenosphere material and interlayer coupling. If these effects compensate each other during some stages of rift evolution, then the resulting net subsidence rate in these stages remains close to that inferred from the commonly inferred thermal model of *McKenzie* [1978], explaining why observed subsidence can be fit by this model in many areas [e.g., *White and McKenzie*, 1988]. Yet any misbalance between these above factors yields strong deviations from the "common" behavior. Even though the model is capable of explaining many known complexities of basin evolution without the necessity of evoking external mechanisms such as phase transitions or inversion of the tectonic stresses and eustasy, it still does not preclude the possibility that the external processes do take their part in a number of situations.

Appendix A: Numerical Model

Figure 1c presents setups for different numerical models based on the finite-element code Parovoz [*Polyakov et al.*, 1993]. The size of the mesh elements varied from 250 m × 250 m to 500 m × 500 m. Parovoz allows for mixed brittle, elastic, viscous, and non-Newtonian temperature-, stress- and strain-rate-dependent power law rheology and complex geometrical structures. This method belongs to the fast lagrangian analysis of continua (FLAC) family [*Cundall and Board*, 1988; *Cundall*, 1989] of large strain fully explicit time-marching numerical algorithms exploiting the Lagrangian " moving grid " method. The latter allows for solution of Newton's equation of motion in large strain mode holding a locally symmetric small strain formulation commonly used in continuum mechanics. The method can reproduce initialization and evolution of nonpredefined faults (treated as large shear bands), which is crucial for the goals of the given study. This algorithm was described by *Cundall* [1989] and *Poliakov et al.* [1993]. Additional details on its later geodynamic version can be found in *Burov and Guillou-Frottier* [1999].

The code solves Newton equations of motion in continuum mechanics formulation:

$$\rho \partial v_i/\partial t - \partial \sigma_{ij}/\partial x_j - \rho g_i = 0.$$

where v is velocity, g is the acceleration due to gravity, and ρ is the density. Solution for velocities at mesh points is used to calculate element strains ε_{ij}. These strains are employed in the constitutive relations yielding element stresses σ_{ij} and equivalent forces $\rho \partial v_i/\partial t$, which provide input for the next calculation cycle. To allow for explicit solution of the governing equations, the algorithm employs a dynamic relaxation technique based on the introduction of artificial inertial masses in the dynamic system. The adaptive remeshing technique permits handling of strain localizations resulting in formation of faults. This method does not imply inherent rheology assumptions, in contrast with common finite element techniques.

A1. Faulting and Continuity

It is very difficult to localize and create "real" discontinuous faults in continuum plasticity code. As was shown by *Cundall* [1990], in most cases that are relevant to our study they can be effectively replaced by plastic shear bands at a price of using a fine numerical grid. The continuum model allows the capture of essential mechanisms that occur in the early stages of localization, in which isolated spots of yielding coalesce to form distinct bands which may then interact with one another. When there is no imposed stress concentrations, the formation of a shear band may be triggered by arbitrary small variations in stress or material properties. For example, in case of plastic rheology, every element in the numerical grid may be given a slightly different value of friction angle (<2°) drawn at random from normal distribution with a mean friction angle (30°). For our study (mixed rheology) it was more convenient to introduce an equally small chaotic variation in the geometry of the elements. The numerical tests for uniaxial deformation and elastic/perfectly plastic rheology with zero cohesion have shown that the shear bands form at angles (θ) very close to theoretical predictions of $\pi/4+\psi/2 < \theta < \pi/4 + \phi$,

where ψ is dilatancy and ϕ is the friction angle [*Cundall*, 1990].

A2. Thermal Model

The mechanical properties and density are temperature-dependent, and the mechanical balance equations are coupled with heat transport equations:

$$div(\mathbf{k}\nabla T)-\rho C_p \partial T/\partial t+H_r = \mathbf{v}\nabla T,$$

where $\mathbf{v}$ is velocity tensor, C_p is the specific heat, $\mathbf{k}$ is the thermal conductivity tensor, H is radiogenic heat production per unit volume (here we use the commonly inferred values adopted, e.g., by *Burov and Diament* [1995] (Table 1). Technically, solutions of the right-hand side (diffusive) and left-hand side (advective) are separated: the latter is calculated automatically when solving the equations of motion, whereas the former is computed using a separate procedure.

Acknowledgments. We greatly benefited from highly useful constructive comments by C. Ebinger and a second, anonymous, reviewer, as well as from discussions with Y. Podladchikov, R. Huismans, S. Cloetingh, J. Deverchere, R. Buck, and A.B. Watts. We are particularly thankful to C. Ebinger for improving the English and the general style of the manuscript. The version of Parovoz used is this study was derived from the original source code developed in 1991-1997 with major involvement of Y. Podladchikov, its principal codeveloper, who is deeply thanked for generously sharing his work and permanent availability at later stages. We note that Parovoz was created independently of its commercial (FLAC) and noncommercial homologues.

References

Avouac, J.-P., and E.B. Burov, Erosion as a driving mechanism of intracontinental mountain growth, *J. Geophys. Res.*, *110*, 17,747-17,769, 1996.

Bassi, G., Relative importance of strain rate and rheology for the mode of continental extension, *Geophys. J. Int.*, *122*, 195-210, 1995.

Beaumont, C., P. Fullsack, and J. Hamilton, Erosional control of active compressional orogens, in *Thrust Tectonics*, edited by K.R. McClay, pp. 1-31, Chapman and Hall, New York, 1992.

Bechtel, D., D.W. Forsyth, V.L. Sharpton, and R.A.F. Grieve, Variations in effective elastic thickness of the North American lithosphere, *Nature*, *343*, 636-638, 1990.

Bertotti, G., Y. Podladchikov, and A. Daehler, Dynamic link between the level of ductile crustal flow and style of normal faulting of brittle crust, *Tectonophysics*, *320*, 195-218, 2000.

Brace, W. F., and D. L. Kohlstedt, Limits on lithospheric stress imposed by laboratory experiments, *J. Geophys. Res.*, *85*, 6248-6252, 1980.

Braun, J., and C. Beaumont, A physical explanation of the relation between flank uplifts and the breakup unconformity at rifted continental margins, *Geology*, *17*, 760-765, 1989.

Buck, W. R., Small-scale convection induced by passive rifting: the cause for uplift of rift shoulders, *Earth Planet. Sci. Lett.*, *77*, 362-372, 1986.

Buck, W. R., Modes of continental lithospheric extension, *J. Geophys. Res.*, *96*, 20,161-20,178, 1991.

Buck, W.R., and A.N.B. Poliakov, Abyssal hills formed by stretching oceanic lithosphere, *Nature*, *392*, 272-275, 1998.

Burov, E.B., and S. Cloetingh, Erosion and rift dynamics: new thermomechanical aspects of postrift evolution of extensional basins, *Earth Planet Sci. Lett.*, *150*, 7-26, 1997.

Burov, E. B., and M. Diament, Flexure of the continental lithosphere with multilayered rheology, *Geophys. J. Int.*, *109*, 449-468, 1992.

Burov, E. B., and M. Diament, The effective elastic thickness (T_e) of continental lithosphere: What does it really mean?, *J. Geophys. Res.*, *100*, 3905-3927, 1995.

Burov, E.B., and M. Diament, Isostasy, effective elastic thickness (EET) and inelastic rheology of continents and oceans, *Geology*, *24*, 419-423, 1996.

Burov, E.B. and L. Guillou-Frottier, Thermomechanical behavior of large ash flow calderas, *J. Geophys. Res.*, *104*, 23,081-23,109, 1999.

Burov, E.B., and P. Molnar, Gravity Anomalies over the Ferghana Valley (central Asia) and intracontinental deformation, *J. Geophys. Res.*, *103*,18,137-18,152, 1998.

Carter, N. L., and M. C. Tsenn, Flow properties of continental lithosphere, *Tectonophysics*, *36*, 27-63, 1987.

Chéry, J., F. Lucazeau, M. Daignieres, and J.-P. Vilotte, Large uplift of rift flanks: A genetic link with lithospheric rigidity?, *Earth Planet. Sci. Lett.*, *112*, 195-211, 1992.

Cloetingh, S.A.P.L., M.J.R. Wortel, and N. J. Vlaar, Evolution of passive continental margins and initiation of subduction zones, *Nature*, *297*, 139-142, 1982.

Cundall, P.A., Numerical experiments on localization in frictional materials, *Ing. Arch.*, *59*, 148-159, 1989.

Cundall, P.A., Numerical modelling of joined and faulted rock, in *International Conference on Mechanics of Jointed and Faulted rock, Vienna, April 18-20*, A.A. Balkema, Brookfield, Vt., 1990.

Cundall, P.A., and M. Board, A microcomputer program for modelling large-strain plasticity problems, in *Numerical Methods in Geomechanics, Proceedings of the 6th International Conference on Numerical Methods in Geomechanics*, edited by C. Swoboda, pp. 2101-2108, A.A. Balkema, Brookfield, Vt., 1988.

Déverchère, J., F. Houdry, M. Diament, N.V. Solonenko, and A.V. Solonenko, Evidence for a seismogenic upper mantle and lower crust in the Baikal rift, *Geophys. Res. Lett.*, *18*, 1099-1102, 1991.

Doser, D., and D.R. Yarwood, Deep crustal earthquakes associated with continental rifts, *Tectonophysics*, *229*, 123-131, 1994.

Dunbar, J.A., and D.S. Sawyer, Continental rifting at pre-existing lithospheric weakness, *Nature, 333*, 450-452, 1988.

Ebinger, C., and N. Sleep, Cenozoic magmatism in Africa resulting from impact of one large plume, *Nature*, *395*, 788-791, 1998.

Ebinger, C. J., T. D. Bechtel, D. W. Forsyth, and C. O. Bowin, Effective elastic plate thickness beneath the East African and Afar Plateaux and dynamic compensation of the uplifts, *J. Geophys. Res.*, *94*. 2883-2901. 1989.

Ebinger, C. J., G. D. Karner, and G. D. Weissel, Mechanical strength of extended continental lithosphere: Constraints from the western rift system, Africa, *Tectonics*, *10*, 1239-1256, 1991.

Ebinger, C., J. Jackson, A. Foster, N. Hayward, Extensional basin geometry and the elastic lithosphere, *Philos. Trans R. Soc. London, Ser. A*, *357*, 741-762, 1999.

England, P., Constraints on extension of the continental lithosphere, *J. Geophys. Res.*, *88*, 1145-1152, 1983.

England, P., and S. W. Richardson, Erosion and the age dependence of the continental heat flow, *Geophys. J. R. Astron. Soc.*, *62*, 421-437, 1980.

Fleitout, L., and C. Froidevaux, Tectonics and topography for a lithosphere containing density heterogeneities, *Tectonics, 1*, 21-57, 1982.

Forsyth, D. W., Finite extension and low-angle normal faulting, *Geology*, *20*, 27-30, 1992.

Gerbault, M., E.B. Burov, A. Poliakov, and M. Dagnieres, Do faults trigger folding in the lithosphere?, *Geophys. Res. Lett., 26*, 271-274, 1999.

Gossman, H., Slope modelling with changing boundary conditions-effects of climate and lithology, *Z. Geomophol., Suppl. 25*, 72-88, 1976.

Hopper, J. R., and W. R. Buck, The effect of lower crustal flow on continental extension and passive margin formation, *J. Geophys. Res.*, *101*, 20,175-20,194, 1996.

Huismans, R.S., Y.Y. Podladchikov, and S.A.P.L. Cloetingh, The transition from passive to active rifting: Relative importance of asthenospheric doming and passive extension of the lithosphere, *J. Geophys. Res.*, in press, 2001.

Karner, G.D., and A.B. Watts, On isostasy at Atlantic-type continental margins, *J. Geophys. Res.*, *87*, 2923-2948, 1982.

Kaufman, P. S., and L. H. Royden, Lower crustal flow in an extensional setting: Constraints from the Halloran Hills region, eastern Mojave Desert, California, *J. Geophys. Res., 99*, 15,723-15,739, 1994.

Kirby, S. H., and A. K. Kronenberg, Rheology of the lithosphere: Selected topics, *Rev. Geophys., 25*, 1219-1244, 1987.

Kirkby, M. J., A two-dimensional model for slope and stream evolution, in *Hillslope Processes*, edited by A.D. Abrahams, pp. 203-224, Allen and Unwin, Concord, Mass., 1986.

Kohlstedt, D. L., B. Evans, and S. J. Mackwell, Strength of the lithosphere: Constraints imposed by laboratory experiments, *J. Geophys. Res.*, *100*, 17,587-17,602, 1995.

Kooi, H., and C. Beaumont, Escarpment evolution on high-elevation rifted margins: Insights derived from a surface processes model that combines diffusion, advection and reaction, *J. Geophys. Res.*, *99*, 12,191-12,210, 1994.

Kusznir, N., G.D. Karner, and S.S. Egan, Geometric, thermal and isostatic consequences of detachments in continental lithosphere extension and basin formation, in *Sedimentary Basins and Basin Formation Mechanisms*, edited by C. Beaumont and A.J. Tankard, *Mem. Can. Soc. Pet. Geol., 12*, 185-203, 1987.

Lavier, L.L., and M.S. Steckler, The effect of sedimentary cover on the flexural strength of the continental lithosphere, *Nature*, *389*, 476-479, 1997.

Lavier, L.L., W.R. Buck, and A.N.B. Poliakov, Factors controlling normal fault offset in ideal brittle layer, *J. Geophys. Res., 105*, 23,431-23,442, 2000.

Leeder, M. R., Denudation, vertical crustal movements and sedimentary basin infill, *Geol. Rundsch.*, *80*, 441-458, 1991.

Lobkovsky, L. I., and V. I. Kerchman, A two-level concept of plate tectonics: Application to geodynamics, *Tectonophysics*, *199*, 343-374, 1992.

McKenzie, D., Some remarks on the development of sedimentary basins, *Earth Planet. Sci. Lett.*, *40*, 25-32, 1978.

Olsen, K. H., *Continental Rifts: Evolution, Structure, Tectonics, Dev. Geotect.*, vol. 25, Elsevier Sci., New York, 1995.

Petit, C., E.B. Burov, and J. Deverchere, On the structure and the mechanical behaviour of the extending lithosphere in the Baikal rift from gravity modeling, *Earth Planet Sci. Lett.*, *149*, 29-42, 1997.

Poliakov, A.N.B., Y. Podladchikov, and C. Talbot, Initiation of salt diapirs with frictional overburden: Numerical experiments, *Tectonophysics*, *228*, 199-210, 1993.

Poliakov, A.N.B., Y.Y. Podladchikov, and D.A. Yuen, A model of sedimentary basin formation with phase-transition and erosion: explanation of synrift uplift and stratigraphic onlap, *Tectonophysics*, in press, 2001.

Ranalli, G., *Rheology of the Earth*, 413 pp., Chapman and Hall, 2nd ed., New York, 1995.

Rohrman, M., P. van der Beek, P. Andriessen, and S. Cloetingh, Meso-Cenozoic morphotectonic evolution of southern Norway: Neogene domal uplift inferred from apatite fission track thermochronology, *Tectonics*, *14*, 704-718, 1995.

Royden, L., and C. E. Keen, Rifting process and thermal evolution of the continental margin of eastern Canada determined from subsidence curves, *Earth Planet. Sci. Lett.*, *51*, 343-361, 1980.

Salveson, J.O., Variations in the geology of rift basins: A tectonic model, *Conf. Proc. Los Alamos Natl. Lab.*, *7487*, pp. 82-86, Los Alamos, N.M., 1978.

Stephenson, R. A., S. M. Nakiboglu, and M. A. Kelly, Effects of asthenosphere melting, regional thermoisostasy, and sediment loading on the thermomechanical subsidence of extensional sedimentary basins, in *Origin and Evolution of Sedimentary Basins and Their Energy and Mineral Resources*, *Geophys. Monogr. Ser.*, vol. 48, edited by R.A. Price, pp.17-27, AGU, Washington, D.C., 1989.

Turcotte, D. L., and G. Schubert, *Geodynamics. Applications of Continuum Physics to Geological Problems*, 450 pp., John Wiley, New York, 1982.

van Balen, R., P. A. van der Beek, and S.A.P.L. Cloetingh, The effect of rift shoulder erosion on stratal patterns at passive margins: Implications for sequence stratigraphy, *Earth Planet. Sci. Lett.*, *134*, 527-544, 1995.

van der Beek, P., P. Andriessen, and S. Cloetingh, Morphotectonic evolution of rifted continental margins: Inferences from a coupled tectonic-surface processes model and fission track thermochronology, *Tectonics*, *14*, 406-421, 1995.

Watts, A. B., and M. Torne, Crustal structure and the mechanical properties of extended continental lithosphere in the Valencia through (western Mediterranean), *J. Geol. Soc. Lond.*, *149*, 813-827, 1992.

White, N., and D. P. McKenzie, Formation of the "Steer's Head" geometry of sedimentary basins by differential stretching of the crust and mantle, *Geology*, *16*, 250-253, 1988.

Willgoose, G., R. L. Bras, and I. Rodrigues-Iturbe, A coupled channel network growth and hillslope evolution model, 1, Theory, *Water Resour. Res.*, *27*, 1671-1684, 1991.

Ziegler, P. A., Geodynamic processes governing development of rifted basins, in *Geodynamic Evolution of Sedimentary Basins, International Symposium*, edited by F. Roure et al., pp. 19-67, Nauka, Moscow, 1994.

E. Burov, Laboratoire Téctonique ESA 7072, Case 129, T26-16, étage 1, Université de Pierre et Marie Curie, 4 Place Jussieu, F-75252 Paris cedex 05, France. (evgenii.burov@lgs.jussieu.fr)

A. Poliakov, Laboratoire de Géophysique, Téctonique et Sédimentologie, CNRS UMR 5573, Université Montpellier II, F-34095 Montpellier cedex 05, France. (aljosha@dstu.univ-montp2.fr)

(Received May 10, 2000; revised December 5, 2000; accepted February 23, 2001.)